2021

# DEVELOPMENT OF MIRIPLATIN-LOADED NANOPARTICLES AGAINST NON-SMALL CELL LUNG CANCER

Zhongyue Yuan
*University of the Pacific*

# DEVELOPMENT OF MIRIPLATIN-LOADED NANOPARTICLES AGAINST NON-SMALL CELL LUNG CANCER

By

Zhongyue Yuan

A Thesis Submitted to the

Graduate School

In Partial Fulfillment of the

Requirements for the Degree of

MASTER OF SCIENCE

Thomas J. Long School of Pharmacy
Pharmaceutical and Chemical Sciences

University of the Pacific
Stockton, California

2021

# DEVELOPMENT OF MIRIPLATIN-LOADED NANOPARTICLES AGAINST NON-SMALL CELL LUNG CANCER

By

Zhongyue Yuan

APPROVED BY:

Thesis Advisor: Xin Guo, Ph.D.

Committee Member: Qinliang Zhao, Ph.D.

Committee Member: Melanie A. Felmlee, Ph.D.

Department Chair: William K. Chan, Pharm.D., Ph.D.

# ACKNOWLEDEGEMENTS

I would like to express my sincere gratitude to many people. The work presented here would not be possible without their help.

I would first and foremost like to thank my advisor Dr. Xin Guo for his continuous guidance and full support during the past three years. It is my distinct pleasure to work with him on this promising project. His enthusiasm and critical thinking always inspired me to be an independent and creative graduate student, researcher, and scientist in the future. I really enjoyed the environment of freedom he established in the lab. During group meeting, we discussed research data without pressure. He aroused and protected my passion of research and encouraged me for further research and study. His advice on both research as well as on my personal life have been invaluable.

I would also thank Dr. Xiaoling Li. He introduced the UOP and the PCSP during his summer international class at China Pharmaceutical University in 2016. When I met the key choices for future study and asked his advice, he always set a meeting to discuss with me and gave excellent suggestions, which have contributed greatly to my research and career. Further, I really appreciate his support for my Ph.D. application and his guidance to develop my leadership in AAPS-UOP student chapter.

I really appreciate Dr. Melanie Felmlee's participation to my thesis committee. Also, she provided lots of help and suggestions in our research. She is an expert in terms of animal technology. I learned so much from her, especially passion and techniques for the scientific research. In the same way, I would like to thank Dr. Qinliang Zhao for the permission and support to work in her lab as well as all help in my research. She is the master of inorganic

chemistry. I learned a lot from her in the field of platinum study. I also appreciated Dr. William K. Chan, Dr. John C. Livesey and Dr. Jianhua Ren for the permission to so many instruments in their labs which greatly supported my research. I want to thank Dr. Fei Guo for using TEM in his department at UC Davis. I also would like to thank UC Davis Interdisciplinary Center for using their Inductively Coupled Plasma Mass Spectrometry. My thanks also go to Lynda, Sonya, Kathy and all PCSP faculty and staff for their taking care during my study life here.

I would like to thank Guo's group members both past and present. Especially thank to Dr. Yifan Lu, Yingbo Huang and Dr. Mallika Vadlamudi, who provided excellent training, valuable suggestions, and lots of help on my project. I also want to thank Zizhao Xu for being my research partner, all his assistance, support, and great discussion with him. I also appreciate Dr. Shen Zhao, Ruiqi Huang, Xinyu Pei, and Yong Zhu for their suggestions, kindness, and support both in my research and life. Thanks Dr. Chao Feng and Yuntao Zhang for their advice and help in my research. I want to thank my friends Hao Wei, Fang Liu, Qing Zhang, Dan Shao, Dengpan Liang, Rui Xiong, Jingda Wang, Michael Ng, Yiyuan Wang, Dr. Yujuan Zheng, Dr. Yujie Yang, Dr. Jinyu Chen, Dr. Jieyun Cao, Pramila Sharma, Md Tariqul Haque Tuhin, Toufiq Ul Amin, Guanming Jiang, Ryan Murray, Shengxi Li, Junyu Chen, Xiaoli Le, Baixue Zhang, Dandi Weng, and Xiaonan Li for their help and the happiness they brought to my memorable life in UOP. Thanks to my friend, Li Zhou, for his countless support and encouragement.

Last, but not least, I would like to thank my parents and family for their unconditional support, endless love, and understanding, which strengthen me to walk through this tough but invaluable journey.

# DEVELOPMENT OF MIRIPLATIN-LOADED NANOPARTICLES AGAINST NON-SMALL CELL LUNG CANCER

## Abstract

By Zhongyue Yuan

University of the Pacific
2021

Lung cancer claims the highest mortality and the second-most estimated new cases among all oncological diseases [1]. Non-small cell lung cancer (NSCLC) accounts for approximately 85% of all newly diagnosed lung cancers [2]. Approximately 40% of newly diagnosed lung cancer patients are stage IV. For stage IIIB/IV NSCLC, cytotoxic combination chemotherapy is standard first-line chemotherapy. A regimen of platinum (Cisplatin or Carboplatin) plus Paclitaxel, gemcitabine, docetaxel, vinorelbine, irinotecan, or pemetrexed is the recommended clinical treatment [3].

Cisplatin is the first-generation platinum-based anti-cancer drug. Although Cisplatin is much more effective than other platinum drugs at the same dosage [4], accumulating reports have shown the failure of conventional platinum-based chemotherapy due to various side effects and drug resistance [5]. Miriplatin, a member of platinum drug family, has been approved in Japan in 2009 for transcatheter arterial chemoembolization treatment of hepatocellular carcinoma (HCC) [6]. Miriplatin is a lipophilic platinum drug that contains myristates (14-carbon chains) as leaving groups and diamino cyclohexane as the non-leaving carrier ligand. The application of Miriplatin in clinic is limited because it has very poor solubilities both in water and in common organic solvents [7].

The structure of solid tumors and tumor microenvironment (TME) in lung cancer constitute a barrier to the deep penetration of chemotherapy agents, which limits the effectiveness of chemotherapy [8]. Nanoparticles with appropriate properties provide a promising delivery system to overcome the biological and physiochemical barriers that hinder anti-cancer activity [9]. Lipid-based nanoparticles such as liposomes, micelles, and solid lipid nanoparticles (SLNs) can delivery anti-cancer drugs to improve their anti-cancer activities. In this study, we formulated Miriplatin into various micelles, liposomes, and SLNs by film-hydration and evaluated their physicochemical properties and anti-cancer activity against NSCLC cells in culture.

Miriplatin-loaded formulations with different compositions were successfully prepared by the film-hydration method. Most Miriplatin-loaded micelles were more homogeneous and much smaller than Miriplatin-loaded liposomes and SLNs. The majority of Miriplatin-loaded micelles were about 15 nm in diameter, while SLNs were around 120 nm, and liposomes were about 180 nm. Formulations with a higher molar ratio of PE-$PEG_{2000}$ had smaller sizes. SLNs loaded with a higher molar ratio of Miriplatin in the compositions showed smaller sizes.

Inductively coupled plasma mass spectrometry (ICP-MS) and inductively coupled plasma optical emission spectrometry (ICP-OES) techniques were attempted to quantify the platinum element in the formulations. Formulations with a higher molar ratio of PE-$PEG_{2000}$ had higher recovery of platinum element. Most Miriplatin-loaded formulations had higher than 80% platinum recovery. The recovery of intact Miriplatin was characterized by HPLC. Miriplatin-loaded micelles had much higher intact Miriplatin recovery (about 100%) than SLNs (about 30%).

By TEM imaging, the micelles showed the morphology of spherical dots of about 10 nm in diameter while SLNs showed both spherical and rodlike structures of about 120 nm in diameter. The TEM results were consistent with the size and PDI results by the Zetasizer.

Three-dimensional multicellular spheroids (3D MCS) of A549 and A549-iRFP cell lines were successfully established as cell culture models to evaluate activity against non-small cell lung cancer. The viability of 3D MCS after 7-days treatment with Miriplatin-loaded micelles was about 0%, which was similar to Cisplatin. Miriplatin-loaded formulations with a higher molar ratio of PE-$PEG_{2000}$ in the compositions had higher anti-cancer activity against 3D MCS. The anticancer activity of Miriplatin-loaded formulations against 3D MCS was positively associated with the recovery of intact Miriplatin from the formulations. The IC50 value of Miriplatin-loaded micelles against A549-iRFP 3D MCS was around 25 μM, while that of Cisplatin was 84.78 μM.

In summary, the reported lipid-based nano-formulations represent a promising delivery system of Miriplatin against NSCLC.

TABLE OF CONTENTS

# LIST OF TABLES

Table

# LIST OF FIGURES

Figure

# LIST OF ABBREVIATIONS

| | |
|---|---|
| AR | aspect ratio |
| CBDCA | 1,1-cyclobutanedicarboxylate |
| CMC | critical micelle concentration |
| DACH | 1R,2R-diaminocyclohexane |
| DLS | dynamic light scattering |
| FDA | Food and Drug Administration |
| HCC | hepatocellular carcinoma |
| HEPES | 4-(2-hydroxyethyl)-1-piperazineethanesulfonic acid |
| HPLC | high performance liquid chromatography |
| ICH | International Conference of Harmonisation |
| ICP-MS | inductively coupled plasma mass spectrometry |
| ICP-OES | inductively coupled plasma-optical emission spectrometry |
| $IC_{50}$ | fifty percent inhibitory concentration |
| iRFP | near-infrared fluorescent protein |
| Miri | Miriplatin |
| NSCLC | non-small cell lung cancer |
| PDI | polydispersity index |
| PEG | polyethylene glycol |
| PE-$PEG_{2000}$ | 1,2-distearoyl-*sn*-glycero-3-phosphoethanolamine-N- [methoxy (polyethylene glycol)-2000] |
| PS | performance status |
| PTX | Paclitaxel |

| | |
|---|---|
| SCLC | small cell lung cancer |
| SLN | solid lipid nanoparticle |
| TEM | transmission electron microscopy |
| TM | trimyristin |
| TME | tumor microenvironment |
| TP | tripalmitin |
| USP | United States Pharmacopeia |
| 2D | two-dimensional |
| 3D MCS | three-dimensional multicellular spheroid |

# CHAPTER 1: INTRODUCTION

## 1.1 Statement of the Problem

### 1.1.1 Non-small Cell Lung Cancer

Lung cancer claims the highest mortality and the second-most estimated new cases among all oncological diseases [1]. The causes of lung cancer are various, including smoking, air pollution, cooking oil and so on. The most common cause is tobacco smoking, accounting for more than 80% of the cases in the United States and other countries where smoking is common [10]. In China, the incidence of lung cancer among nonsmokers is high, and this is particularly notable in women, probably because of ambient air pollution exposure. Also, for female who cooks often, long-term exposure to cooking oil fumes is also one of the causes of lung cancer [11].

Lung cancer is categorized into two main histological groups: small cell lung carcinoma (SCLC) and non-small cell lung cancer (NSCLC) [12]. NSCLC accounts for approximately 85% of all newly diagnosed lung cancers [2]. As shown in Figure 1, NSCLC has three main subtypes, namely adenocarcinoma, squamous cell carcinoma and large-cell carcinoma [12]. Adenocarcinoma accounts for approximately 40% of non-small cell lung cancer cases in which solid tumors tend to develop in the peripheral bronchioles that are usually located on the outer edge of the lung [13]. It is also the most common cancer in women and non-smokers [14]. Squamous cell carcinoma accounts for about 25% of non-small cell lung cancer cases, which are characterized by the presence of intercellular bridges and keratinization [12]. These NSCLCs are associated with smoking and occur predominantly in men [15]. Squamous cell cancers can

present as Pancoast tumor and hypercalcemia [16]. Lastly, large cell carcinoma lacks the differentiation among a small cell, glandular and squamous cells [17].

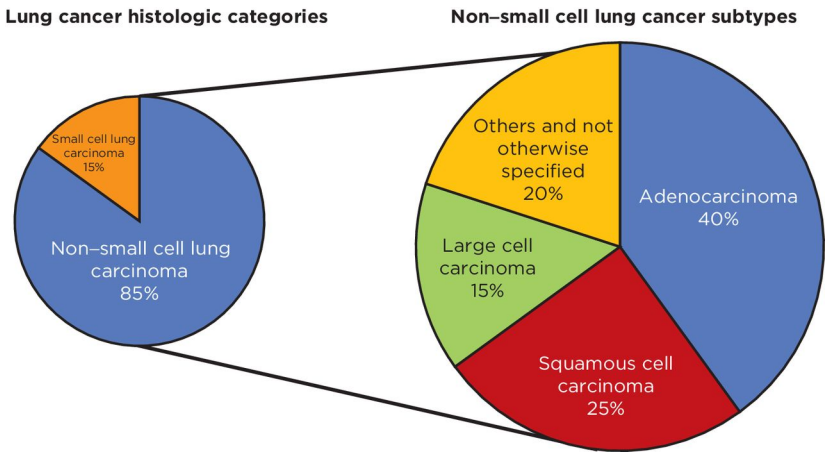


*Figure 1.* Lung cancer classification. Adapted from [18].

### 1.1.2 Treatment Options and Chemotherapy

Treatment options of lung cancer include surgery, chemotherapy or other medications, radiation therapy, local treatments such as laser therapy, or a combination of these treatments. Combination treatment refers to having more than one type of treatment together or successively. Specific treatment for lung cancer depends on its type and stage.

Surgery is part of the treatment for early-stage lung cancers [5]. In stage I, II, and IIIA of NSCLC, the tumor is typically removed by surgery if the tumor is found to be resectable and the patient is healthy enough to tolerate surgery [19]. Patients who have received a resection surgery may benefit from adjuvant therapy (such as radiation, and chemotherapy) in order to reduce the risk of lung cancer relapse. The patients usually receive chemotherapy after surgery in order to kill the remaining cancer cells and to inhibit the inflammation [20].

Patients who are not suitable for surgical resection may benefit from radiotherapy [5]. Radiotherapy also may be included as palliative care to improve the life quality of patients who do not respond to surgery or chemotherapy [21].

Immunotherapy is a breakthrough treatment in oncology. Immunotherapy works by boosting the immune system so that it can target the cancer cells, inhibit the tumor growth, and prevent the cancer metastasis [22].

Approximately 40% of newly diagnosed lung cancer patients are stage IV [5] for which combination chemotherapy is the first-line treatment [5]. The American Society of Clinical Oncology states that the treatment is a regimen of platinum (Cisplatin or Carboplatin) plus Paclitaxel, Gemcitabine, Docetaxel, Vinorelbine, Irinotecan, or Pemetrexed [3]. Results from recent clinical trials have shown that no single regimen demonstrated a significant superiority over any other treatment [23, 24]. The treatment of choice should be decided based on the patient's individual profile, depending on the cancer type, the performance status (PS), and the toxicity [5]. For example, patients with PS of 0 or 1 would take a platinum-based regimen; patients with a PS of 2 may need only one drug, which is usually not platinum [25]; patients with a PS of 3 would not benefit from cytotoxic chemotherapy because of the high risk of adverse toxicity, which would decrease their life quality [5].

### 1.1.3 Platinum-based Anticancer Drugs

With the discovery of Cisplatin and the subsequent expansion of the platinum drug family, the treatment of cancer has been revolutionized. Platinum-based drugs account for approximately 50% of anticancer therapeutic agents in clinic [26]. Cisplatin was first synthesized by Peyrone, M. Ann. 1844 [27]. It is a well-known chemotherapeutic drug that has been used for treatment of numerous human cancers including bladder, head and neck, lung,

ovarian, and testicular cancers [4]. Cisplatin was the earliest platinum drug approved by the United States Food and Drug Administration (FDA) for advanced ovarian and bladder cancer treatment in 1978 [28].

As shown in the Figure 2, the Cisplatin complex moves through cell membranes by passive diffusion, and this is because of the relatively high concentration of chloride in the plasma. Inside the cells the concentration of chloride ions is lower than in the plasma and the chloride ligands on the Cisplatin complex are displaced by water. The displacement yields positively charged platinum complexes that are toxic to cells [26]. Cisplatin's cytotoxicity comes from its interaction with DNA to form DNA adducts, which activate several signal transduction pathways (such as ATR, p53, p73, and MAPK). The cytotoxicity culminates in the inhibition of the synthesis of DNA, RNA, and protein and the activation of apoptosis [29]. However, the clinical application of Cisplatin is limited by drug resistance and toxicity [5, 29]. The mechanisms of Cisplatin resistance include decreased drug uptake, reducing anti-cancer activities, and increased DNA repair [29]. The resistance to Cisplatin is developed by prolonged drug exposure [30]. In addition, Cisplatin-based therapies are challenged by various adverse effects including nausea, nephrotoxicity, cardiotoxicity, hepatotoxicity, ototoxicity, gastrotoxicity, neurotoxicity, myelosuppression, and allergic reactions [31, 32]. The administration of Cisplatin for cancer treatment is highly controlled due to these side effects [31]. Nephrotoxicity is mainly associated with high doses of Cisplatin, so practitioners are suggested to reduce the Cisplatin dosage when a patient's renal function deteriorates [31]. Except nephrotoxicity, most of other common toxicity to normal tissues is caused by the limited selectivity of drugs [33].

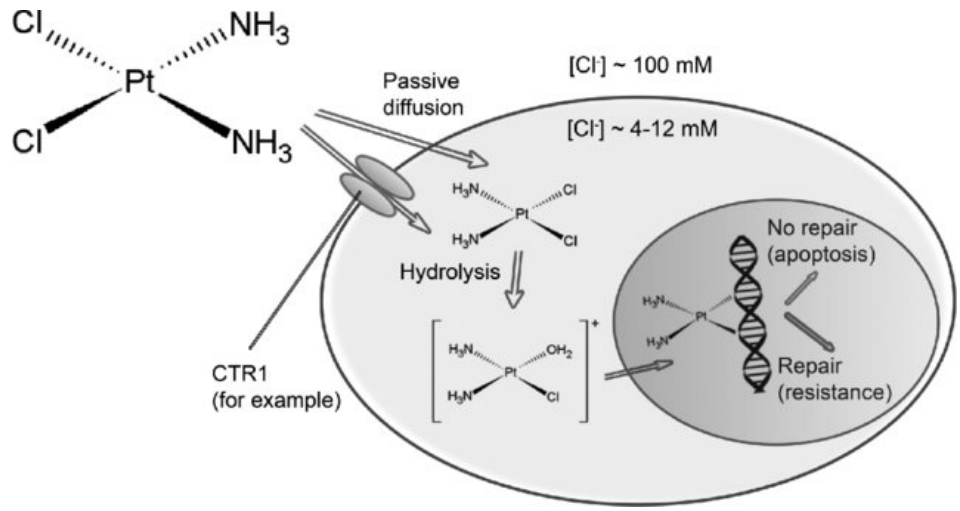


*Figure 2.* Mechanism of Cisplatin action. Adapted from [26].

To overcome drug resistance and to reduce the toxicity of Cisplatin, various platinum complexes have been investigated [34]. The development of new platinum complexes involves modification of the ligands of the platinum complex. As shown in Figure 3, the non-leaving group (ligand L) is usually a nitrogen donor and forms a thermodynamically stable bond with platinum. This non-leaving ligand usually remains unchanged during drug activation and directly affects the properties of the final platinum-DNA adduct [35]. The leaving group (ligand X) is unstable and can be replaced by ligand substitution. The modification of ligand X can change the hydration/activation kinetics, toxicity characteristics and solubility [35]. The replacement of the leaving groups induces the platinum ion to form bonds with DNA bases [4, 36]. Axial ligands R are only found in higher-valent platinum drugs, such as Platinum (III) and Platinum IV) [26, 37].

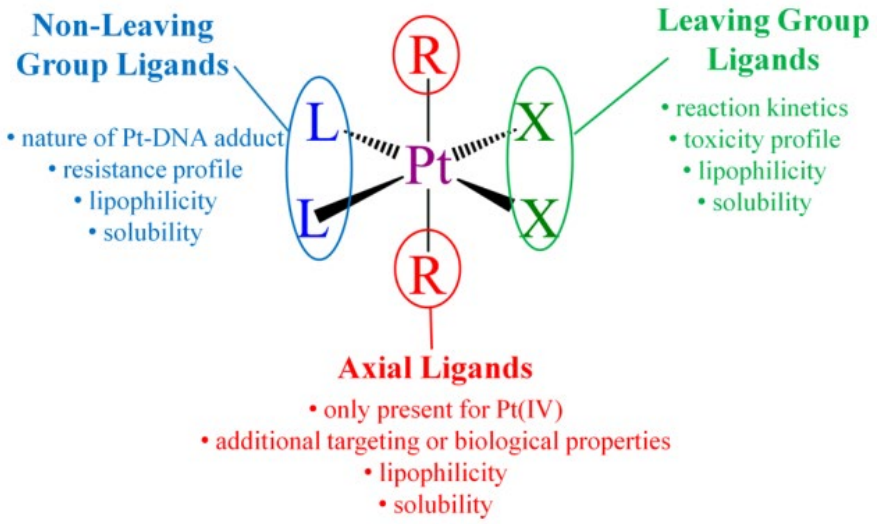


*Figure 3.* General structure of platinum-based anti-cancer drugs. Adapted from [38].

Any modification of these three types of ligands will change the polarity and water-solubility of the platinum complexes. It is important physicochemical parameters for platinum drug's pharmacokinetics and pharmacodynamics [26]. The family tree of platinum complexes is shown in Figure 4. Only Cisplatin and Carboplatin have been approved globally for clinical use. While the other four compounds are approved only for regional use in Asia [39].

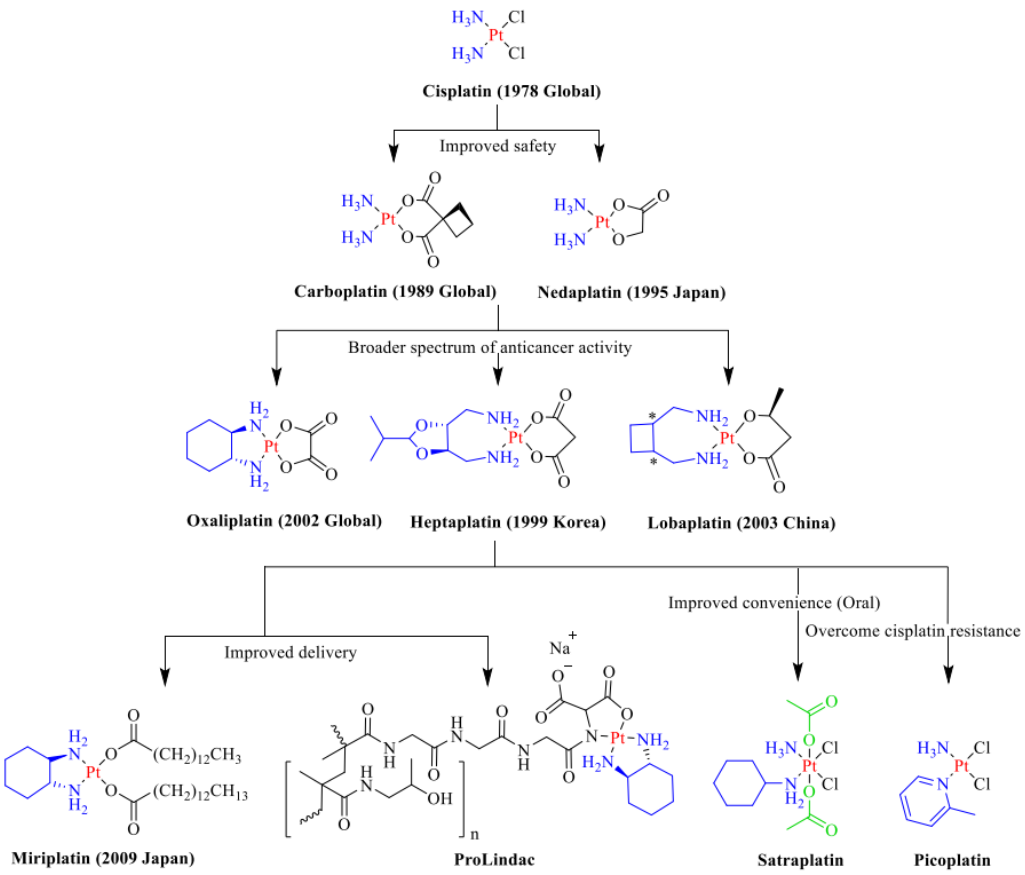


*Figure 4.* The family tree of platinum-based anti-cancer drugs. Adapted from [40].

Carboplatin was approved by FDA as a second-generation platinum-based anti-cancer drug in 1989 [41]. The structure of Carboplatin differs from Cisplatin in that the leaving group is CycloButane DiCarboxylic Acid (CBDCA) instead of the two chloride ligands, which are the leaving groups in Cisplatin [41]. Compared with Cisplatin, Carboplatin needs four-fold higher dosage to achieve similar anti-cancer activity [4]. Carboplatin exhibits cross-resistance with Cisplatin because they have the same non-leaving group [42]. Oxaliplatin has another chelating ligand as a leaving group and a different non-leaving group, 1R,2R-diaminocyclohexane (DACH). Oxaliplatin needs to be activated by replacing the oxalate ligand with chloride ions

[43]. Oxaliplatin is part of the 'DACH' family of platinum compounds. This group yielded promising anti-cancer activity. However, they also caused low water solubility, which limited their clinical application [44].

Miriplatin was approved in Japan for transcatheter arterial chemoembolization treatment of hepatocellular carcinoma [6]. Miriplatin is a lipophilic platinum drug that contains myristates (14-carbon chains) as leaving groups and diamino cyclohexane as the non-leaving carrier ligand. It can be suspended in ethyl esters of iodized fatty acids from poppy seed oil. The Miriplatin suspension is active for local anticancer therapy such as *trans*- arterial chemoembolization and lipodolization. The intact anti-cancer drug that is released from the suspension and selectively retained in hepatocellular carcinoma provides the anticancer effect [45]. Miriplatin possesses very poor solubilities both in water and in common organic solvents, which limits its applications in systemic administration [7].

### 1.1.4 Barrier of Drug Delivery into Solid Tumor

Drug toxicity and drug resistance based on cell culture studies are the main reasons for the limitations of anti-cancer chemotherapy. However, recent studies have indicated that the tumor microenvironment (TME) also contributes to the tumor's resistance against chemotherapy [46]. As shown in Figure 5, the TME is a complex ecosystem consisting of heterogeneous tumor cells, stromal cells, and a variety of immune cells residing in a network of dysregulated vasculature and collagen. Poor perfusion and densely packed glycolytic tumor cells create pockets of diminished oxygen, acidic pH, poor nutrients, anti-inflammatory cytokines, chemokines, and accumulated metabolic by-products. Tumor-infiltrating immune cells of both the myeloid and lymphoid lineages are found within the TME [47]. The vasculature of many solid tumors is poorly developed, the blood flow rate is unstable, and the distance between

capillaries is much greater than that of the vasculature in normal tissues [8]. Penetration into the tumor tissue from the blood vasculature is also required for the efficacy of anticancer agents against solid tumors. Therefore, the limited penetration prevents most cancer cells from being exposed to lethal concentrations of anticancer drugs, especially cancer cells in the hypoxic core of solid tumors [8]. In addition, hypoxia is involved in the resistance against many anti-cancer drugs [48]. As solid tumors have a poor vasculature due to their rapid growth, there is a substantial diffusion barrier between the drug supply vessel and tumor cells [49]. In summary, several characteristics of solid tumors constitute a physiochemical barrier for uniform distribution and deep penetration of chemotherapy agents.

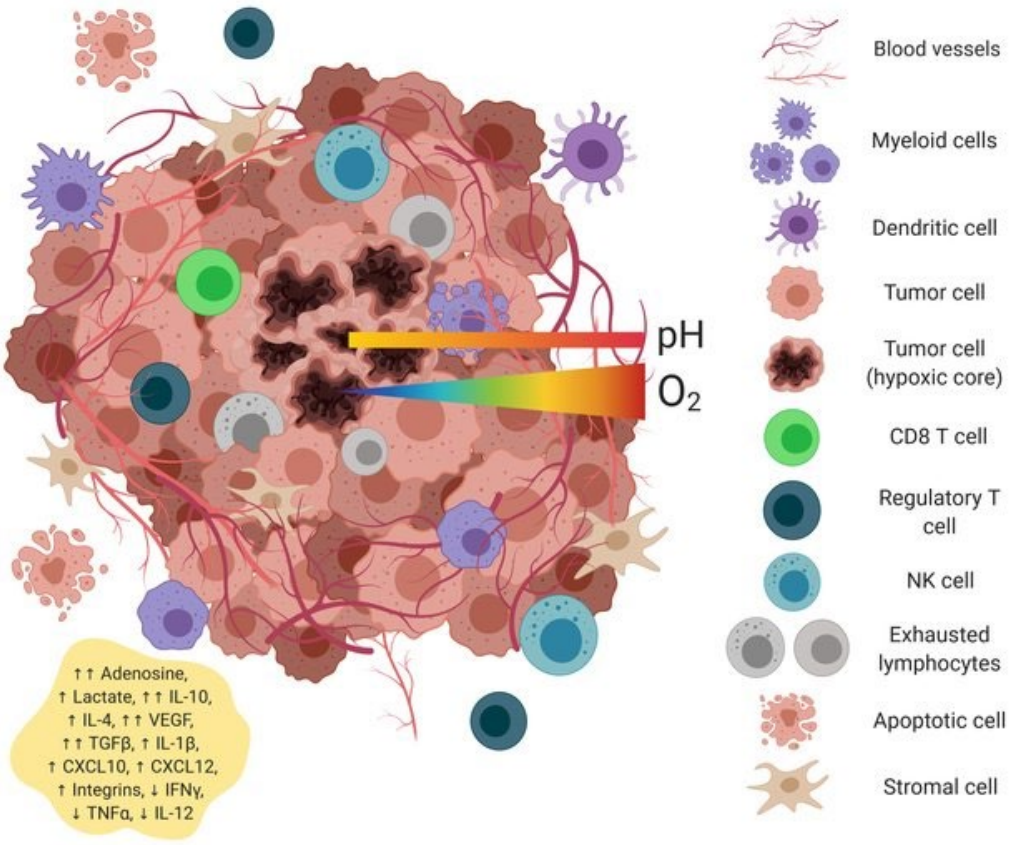


*Figure 5.* Components of the tumor microenvironment. Adapted from [47].

## 1.2 Lipid-based Nanoparticles

As defined by the FDA, nano-formulations are products in combination with nanoparticles ranging between 10 to 100 nm in diameter or other formulations outside of this size range with dimension-dependent properties [50]. These formulations exhibit many advantages over free drug molecules, including enhanced solubility, improved pharmacokinetics, better efficacy, and lower toxicity [50]. Lipid-based nanoparticles have played a pivotal role in the successes of COVID-19 vaccines and many other nanomedicines (such as Doxil® and Onpattro®) and have therefore been considered as the frontrunner among nanoscale drug delivery systems [51].

Lipid nanoparticles are multi-component lipid systems, usually containing phospholipids that form bilayer structures, auxiliary lipids that improve cell binding, cholesterol and surfactants that fill structural gaps, and Polyethylene glycol (PEG)-lipid conjugates that decrease serum protein adsorption and thus decrease reticuloendothelial clearance [51]. Based on the lipid composition and the nano-sized structure, lipid-based nanoparticles mainly include micelles, liposomes, and solid lipid nanoparticles (SLNs) (Figure 6).

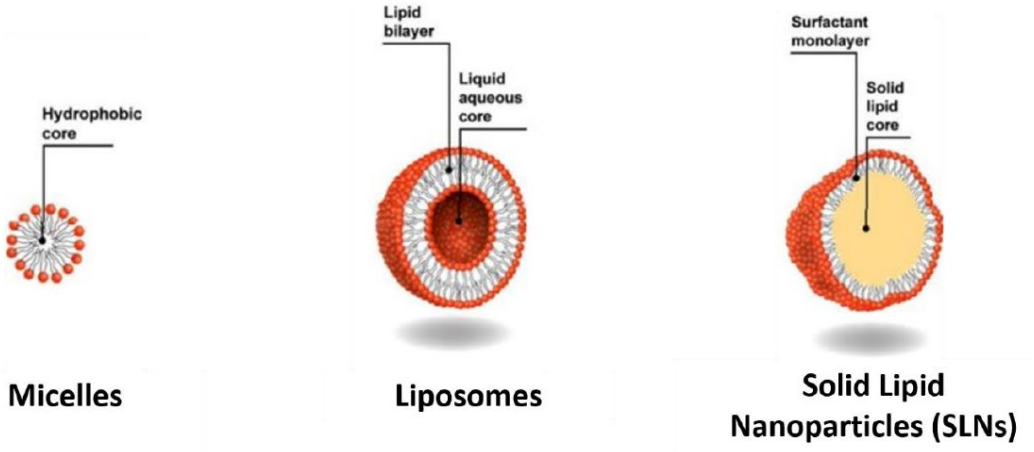


*Figure 6.* Examples of lipid-based nanoparticles: micelles, liposomes and solid lipid nanoparticles (SLNs). Adapted from [52].

### 1.2.1 Liposomes

Liposomes are the most commonly used nanocarriers. Most of the anticancer nanomedicines approved by the FDA are based on liposome structures [53]. Liposomes are mainly composed of phospholipids and have a lipid bilayer shell encapsulating an aqueous interior. Liposomes can be loaded with both lipophilic and hydrophilic drug molecules [54]. Liposomes were first described in 1961 by the British haematologist, Alec D Bangham [55]. Liposomes have a size ranging from 50 to 500 nm in diameter. Liposomes with an average diameter between 100 and 150 nm can enter the liver endothelium, secondary lymphatic structure or porous blood vessels in TME [56]. In addition, liposomes with a diameter of 100-150 nm can be better taken up by cells through endocytosis [57].

### 1.2.2 Micelles

Micelles are spherical colloids, composed of a core of nonpolar groups of its surfactant monomers and a surface of polar head groups of the same surfactant monomers[58]. Compared to liposomes, micelles have a smaller size, ranging from 10 nm to 100-200 nm [58]. The

extremely small size of micelles might be beneficial to tumor penetration and accumulation [59, 60]. Researchers developed polymer micelles loaded with 1,2-diaminocyclohexane-platinum (II) with a diameter of 30 nm. Such micelles can accumulate and penetrate in poorly permeable pancreatic tumors without any targeting ligands [61]. However, the accumulation and blood circulation time of micelles improved with larger size with optimal diameter range of 100 to 160 nm [62].

### 1.2.3 Solid Lipid Nanoparticles (SLNs)

SLNs possess a hydrophobic core of solidified lipid molecules. SLNs carry a size ranging from 10 to 1000 nm in diameter [63]. The major components of SLNs are solid lipids such as triglycerides (tri-stearin), partial glycerides (Imwitor), fatty acids (stearic acid, palmitic acid), steroids (cholesterol), and waxes (cetyl palmitate). Various emulsifiers and their combinations have been used to stabilize the SLN dispersion [64]. Compared to micelles and liposomes, SLNs in general provide better stability and prolonged release [65].

## 1.3 Hypothesis and Specific Aims

Based on the foregoing, it is hypothesized that Lipid-based formulations of Miriplatin would carry appropriate physiochemical properties to improve the anticancer activity of platinum drugs against non-small cell lung cancer. To test the hypothesis, the research of this thesis focusses on the following specific aims:

1. To develop Miriplatin-loaded formulations and optimize their lipid composition.
2. To characterize the physiochemical properties and morphology of Miriplatin-loaded formulations.
3. To evaluate the anticancer activity of Miriplatin-loaded formulations in three-dimensional multicellular spheroids (3D MCS).

# CHAPTER 2: PREPARATION OF LIPID-BASED NANO FORMULATIONS OF MIRIPLATIN

## 2.1 Introduction

Lipid-based nanoparticles such as liposomes, micelles, and solid lipid nanoparticles are colloidal nanoparticles made of amphiphilic lipid molecules, which possess both hydrophilic heads and lipophilic tails [66]. Lipid-based nanoparticles can entrap anti-cancer drugs to improve their water solubility and bioavailability [66]. Lipid-based nanoparticles are taken up by cells through endocytosis. Additionally, lipid-based nanoparticles usually contain multiple lipidic components including phospholipids that form bilayer structures, auxiliary lipids that improve cell binding, cholesterol and surfactants that fill structural gaps, and Polyethylene glycol (PEG)-lipid conjugates that decrease serum protein adsorption and thus decrease reticuloendothelial clearance. The composition and of lipid-based nanoparticles significantly affects their delivery efficiency and needs to be optimized for a given application. Furthermore, the physicochemical properties of lipid nanoparticles such as size, and surface charge can influence both their pharmacokinetics and their efficacy in vivo [67].

### 2.1.1 Methods to Prepare Lipid-based Nanoparticles

Various methods to prepare lipid-based nanoparticles have been developed. For examples, thin film hydration, solvent evaporation, ethanol injection, cold/hot homogenization, high speed homogenization, and microfluids are commonly used to prepare different types of nanoparticles in laboratory or industry.

In small laboratory scale, thin-film hydration, aka the Bangham method is one of the simplest and yet most widely used preparation techniques for lipid-based nanoparticle [68, 69].

In this method, a mixture of lipids and drugs is first dissolved in organic solvent(s) and the solution is evaporated under vacuum to obtain a thin layer of lipid film deposited at the bottom of flask. Water or hydration buffer is then added under agitation in a water bath with temperature above the lipid transition temperature (Tm) [68, 70]. The film-hydration method produces large, heterogeneous multilamellar vesicles that need sonication or extrusion processes to yield small, homogeneous unilamellar vesicles [71]. The payload drug molecules can either be encapsulated in the aqueous interior (for hydrophilic drugs) or incorporated into the lipid membrane (for lipophilic drugs) of the lipid nano formulation. Thin film hydration can yield multilamellar vesicles ranging 50–1000 nm in diameter. Due to small production capacity and the presence of organic solvents, thin film hydration has limited application on a commercial scale. Nevertheless, this method has important advantages such as simplicity, high encapsulation efficiency of diverse drugs, and ability to produce small, homogeneous particles [72]. Therefore, thin-film hydration has been used as a quick and simple method to develop optimal lipid compositions in research laboratories [72].

In industry, solvent injection is a commonly used method to scale up the preparation of lipid-based nanoparticles [73]. Generally, a solution of lipids in organic solvent(s) (e.g. ether, ethanol) is injected into an aqueous phase at a temperature above the lipid transition temperature [74]. The main relevance of the solvent injection method lies on the possibility to yield small nanoparticles with narrow size distribution simply by injection [75]. Some modified solvent injection methods have been applied to large-scale production of lipid-based nanoparticles [76]. However, it must be assured that the residual organic solvent is completely removed before the nanoparticles are administered to the patient in order to prevent tissue damages [77].

In addition, other advanced preparation technologies, such as spray drying, cold/hot homogenization, high-speed homogenization, and microfluidics, have also emerged to meet diverse needs of preparation at laboratory and industrial scales. Recently, our research group have also established a solvent injection and evaporation method to prepare lipid-based nanoparticles.

In this study, the thin-film hydration method was established to prepare lipid-based nanoparticles of Miriplatin.

### 2.1.2 Components of Lipid-based Nano Formulations of Miriplatin

The payload drug in this study is Miriplatin, which is an analog of oxaliplatin. Miriplatin was approved in Japan in 2009 for transcatheter arterial chemoembolization treatment of hepatocellular carcinoma [45]. Miriplatin is a highly lipophilic platinum that contains myristates (14-carbon chains) as leaving groups and diamino cyclohexane as a carrier ligand. It can be easily suspended in ethyl esters of iodized fatty acids from poppy seed oil. The Miriplatin suspension is active for local anticancer therapy such as trans arterial chemoembolization and lipodolization. The anticancer drug that is released from the suspension and selectively retained in hepatocellular carcinoma provides the anticancer effect [45]. Miriplatin possesses very poor solubilities both in water and in common organic solvents, which limits its application in systemic administration [7]. The two 14-carbon chains affect the solubility of Miriplatin. Miriplatin can be considered both as an anticancer payload drug but also a lipid component of lipid-based nanoparticles.

Combination therapy is a treatment in which two or more therapeutic drugs are combined together or performed sequentially. This is a key strategy for the treatment of most cancers [78]. Compared with monotherapy, the combination of anticancer drugs can achieve better efficacy,

less drug resistance and lower drug toxicity in clinic [79]. As anticancer chemotherapy regimens, platinum-based drugs (Cisplatin or Carboplatin) combined with Paclitaxel (PTX) are commonly used as first-line treatment of non-small cell lung cancer [23, 80]. In this study, Paclitaxel will also be formulated in combination with Miriplatin in lipid-based nanoparticles. Paclitaxel is a hydrophobic chemotherapy drug to treat numerous types of cancer, including breast cancer, lung cancer, ovarian cancer. Paclitaxel has been readily formulated into lipid-based nanoparticles, such as micelles, liposomes and solid lipid nanoparticles (SLN), which improved its solubility, stability, and safety [81-83]. In the past two decades, several Paclitaxel nano formulations were approved for clinical use [82, 84]. Tripalmitin (TP) or Trimyristin (TM) are triglycerides derived from the palmitic acid and myristic acid, respectively. The SLNs consisting of TP or TM in the solid lipid core have been heavily studied for chemotherapy and immunotherapy [85-87]. Furthermore, Paclitaxel has been successfully formulated into SLNs that consist of tripalmitin and trimyristin [87, 88]. As TP and TM carry hydrocarbon chains that are similar to those of Miriplatin, we aim to formulate Miriplatin into SLNs consisting of TP and TM to enhance its biocompatibility and physical stability.

18:0 PE-$PEG_{2000}$ is a common component of lipid-based nano- drug formulations. 18:0 PE-$PEG_{2000}$ provides a hydrophilic coating on the surface of the drug formulation to hinder the adsorption of serum proteins and thus the clearance by the reticuloendothelial system, thereby prolonging the circulating plasma half-life of the drug formulation.

The objective of this chapter is to develop Miriplatin-loaded formulations and optimize their lipid composition. In this chapter, numerous Miriplatin-loaded lipid-based nanoparticles such as micelles, liposomes, and solid-lipid nanoparticles were developed by thin-film hydration. The size and polydispersity index (PDI) of the nanoparticles were characterized. The micelles

were prepared with 18:0 PE-$PEG_{2000}$; the liposomes were prepared with 16:0 PC (DPPC), 18:0 PE-$PEG_{2000}$, and cholesterol; the SLNs were prepared with TP and/or TM and 18:0 PE-$PEG_{2000}$. Miriplatin, Paclitaxel, and their combination were used as the payload of the nanoparticles. Excipients such as Tween 20, Tween 80, and lecithin were also used to improve the nanoparticles' physicochemical properties such as size, PDI, and drug-loading capacity.

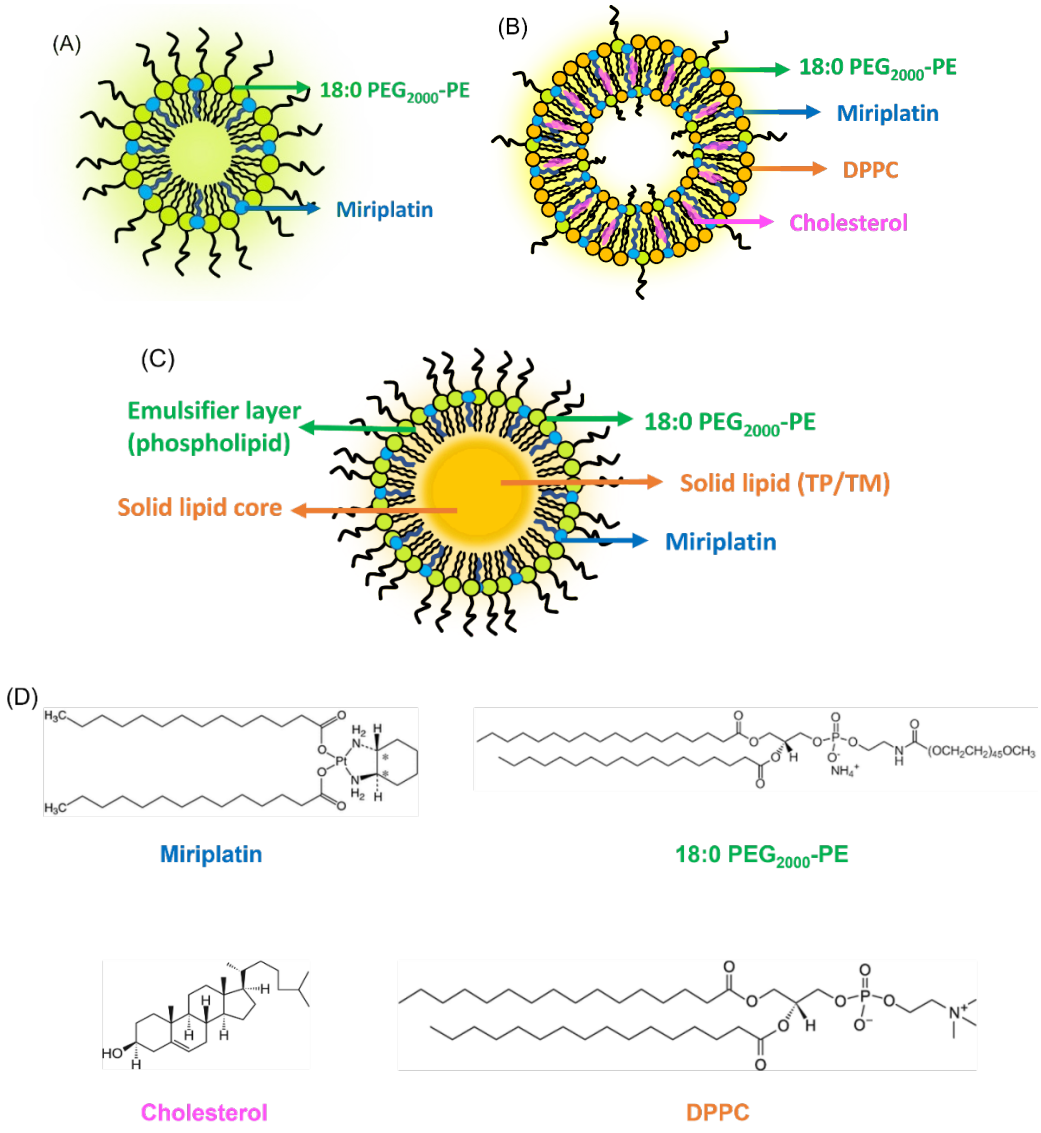


*Figure 7.* Structure of (A) Miriplatin-loaded micelles, (B) Miriplatin-loaded liposomes, (C) Miriplatin-loaded SLNs, (D) Chemical structure for each component.

## 2.2 Materials and Methods

### 2.2.1 Materials

Miriplatin was purchased from MedChem Express LLC (NJ, US). Paclitaxel was purchased from LC Laboratory (MA, US) Cholesterol, Glyceryl tripalmitate, and Glyceryl trimyristate were purchased from Sigma-Aldrich (MO, US). 1,2-distearoyl-sn-glycero-3-phosphoethanolamine-N- [methoxy (polyethylene glycol)-2000] ammonium salt (18:0 PE-$PEG_{2000}$) was purchased from Avanti Polar Lipids, Inc. (AL, USA). 2-[4-(2-hydroxyethyl) piperazin-1-yl]-ethane sulfonic acid (HEPES), Tween 20, and Tween 80 were purchased from Fisher Scientific. Lecithin was purchased from MP Biomedicals (OH, US). All other organic solvent and chemicals were purchased from Sigma Aldrich, Fisher Scientific or VWR.

### 2.2.2 Preparation of Miriplatin-Loaded Formulations by Thin-film Hydration

Various lipids and anticancer drugs were separately dissolved in chloroform for short-term stock. Generally, 0.8 µmol Miriplatin was then mixed with 4 µmol lipidic excipients including lipids, cholesterol, and surfactants in a 25 ml round bottom tube at different molar ratios as shown in Table 1, Table 2, and Table 3. The chloroform solution in the tube was then evaporated in a rota-vaporation at about 60℃. A thin lipidic film was formed after 10 min of continuous evaporation and was placed under high vacuum overnight to remove residual solvent. The hydration buffer (5 mM HEPES, 150 mM NaCl, pH 7.4) and the tube with thin film were pre-heated in a 65 ℃-water bath for 5 min. Then 200 µl hydration buffer was added and mixed with the thin film. The tube was filled with argon and sealed with parafilm to avoid oxidation. Then the film was hydrated in a water bath at 78 ℃ for 45 min. The Miriplatin-loaded micelles were stored at room temperature (25℃) or 4℃. The selected micelles were pre-frozen in liquid

nitrogen for 30 minutes, and then lyophilized overnight at -83℃ under a vacuum of 0.110 mbar. DI water was added to reconstitute the lyophilized micelles.

Table 1
*Composition of Miriplatin-loaded Lipid-based Nanoparticles: Micelles*

| Compositions (molar ratios) | | | |
|---|---|---|---|
| PE-$PEG_{2000}$ | Miriplatin | Paclitaxel | Lecithin |
| 10 | - | - | - |
| 10 | 1 | - | - |
| 10 | 1.5 | - | - |
| 10 | 2 | - | - |
| 10 | 2.5 | - | - |
| 10 | - | 1 | - |
| 10 | - | 2 | - |
| 10 | 1 | 1 | - |
| 10 | 1.5 | 1 | - |
| 10 | 2 | 1 | - |
| 10 | 2.5 | 1 | - |
| 10 | 2 | - | 0.5 |
| 10 | 2 | - | 1 |
| 10 | 5 | - | 4 |

Table 2
*Composition of Miriplatin-loaded Lipid-based Nanoparticles: Liposomes*

| Compositions (molar ratios) | | | |
|---|---|---|---|
| 16:0 PC(DPPC) | Cholesterol | PE- $PEG_{2000}$ | Miriplatin |
| 15 | 4 | 1 | - |
| 15 | 4 | 1 | 2 |
| 15 | 4 | 1 | 4 |
| 15 | 4 | 1 | 8 |

Table 3

*Compositions of Miriplatin-loaded Lipid-based Nanoparticles: SLNs*

| Compositions (molar ratios) | | | | Other Components | | | |
|---|---|---|---|---|---|---|---|
| TP/TM | PE- $PEG_{2000}$ | Miri | PTX | Lecithin | Cholesterol | Tween 20 | Tween 80 |
| 39 | 1 | - | - | - | - | - | - |
| 39 | 1 | 4 | - | - | - | - | - |
| 38 | 2 | - | - | - | - | - | - |
| 38 | 2 | 4 | - | - | - | 1.5% (v/v) | - |
| 38 | 2 | 4 | - | - | - | - | 1% (v/v) |
| 36 | 4 | - | - | - | - | - | - |
| 36 | 4 | 4 | - | - | - | - | 1% (v/v) |
| 36 | 4 | 4 | - | - | - | - | - |
| 36 | 4 | 8 | - | - | - | - | - |
| 36 | 4 | 12 | - | - | - | - | - |
| 36 | 4 | 8 | 4 | - | - | - | - |
| 32 | 8 | 4 | - | - | - | - | - |
| 24 | 16 | - | - | - | - | - | - |
| 24 | 16 | 4 | - | - | - | - | - |
| 24 | 16 | 8 | - | - | - | - | - |
| 24 | 16 | 8 | 4 | - | - | - | - |
| 24 | 16 | 8 | - | 2 | - | - | - |
| 24 | 16 | 8 | - | 4 | - | - | - |
| 24 | 16 | 8 | - | - | 4 | - | - |
| 24 | 16 | 8 | 4 | - | 4 | - | - |
| TP:TM= 18:18 | 4 | 8 | 4 | - | - | - | - |
| TP:TM= 12:12 | 16 | 8 | 4 | - | - | - | - |

(TP: tripalmitin, TM: trimyristin, Miri: Miriplatin PTX: Paclitaxel)

### 2.2.3 Physicochemical Characterizations of Miriplatin-Loaded Formulations

The size and Polydispersity Index (PDI) of the Miriplatin-loaded formulations were characterized by dynamic light scattering using Zetasizer ZS 90 (Malvern Instruments Ltd., Malvern, UK). Miriplatin-loaded formulations (1.5 µl) diluted with 150 µl deionized water was transferred into a low volume cuvette (ZEN0118, Malvern Instruments) and the hydrodynamic diameter was measured in triplicate.

## 2.3 Results and Discussion

### 2.3.1 Sizes and PDI of Miriplatin-loaded Micelles

**2.3.1.1 Effect of different ratios of drug-loading.** Micelles loaded with Miriplatin at different molar ratios were prepared by thin-film hydration and characterized by dynamic light scattering. The resultant hydrodynamic diameter and PDI values are listed in Table 4. The concentration of total lipids was 400 µM, which served as a reference for the molar ratio of drug loading. As shown in Table 4, the size of micelle without Miriplatin loading (blank micelle) was smaller than those with drug input. As the molar ratio of drug loading increases, the sizes of micelles with same lipid compositions increased. However, as shown in Table 2.2.1, white precipitate was observed when the molar ratios of Miriplatin loading to PE-$PEG_{2000}$ exceeded 2:10, or when the molar ratios of Paclitaxel loading to PE-$PEG_{2000}$ exceeded 1:10. Because the volume of formulation was very limited (200µl) and because some water was evaporated during the hydration process, the Miriplatin concentration probably increased after the preparation, which would then increase the size of micelles that were loaded with high 20 mol% of Miriplatin. Additionally, when the sizes were above 50 nm, most PDI values of micelles were below 0.4, which indicated better homogeneity. Micelles loaded with a combination of Miriplatin and PTX showed similar trends in size and PDI compared to micelles loaded only with Miriplatin.

Table 4

*Size and PDI of Miriplatin-loaded Micelles with Different Ratios of Drug Input*

| Compositions (molar ratios) | | | Size (nm, in number) | PDI |
|---|---|---|---|---|
| PE-PEG$_{2000}$ | Miriplatin | Paclitaxel | | |
| 10 | - | - | 9.75 | 1.000 |
| 10 | 1 | - | 11.24 | 0.579 |
| 10 | 1.5 | - | 11.66 | 0.676 |
| 10 | 2 | - | 12.39 | 0.624 |
| 10 | 2 | - | 122.2 | 0.180 |
| 10 | 2.5*↓ | - | 270.8 | 0.342 |
| 10 | - | 1 | 12.09 | 0.528 |
| 10 | - | 2*↓ | 14.30 | 0.530 |
| 10 | 1 | 1 | 208. 3 | 0.187 |
| 10 | 1.5 | 1 | 11.84 | 0.659 |
| 10 | 2 | 1 | 80.73 | 0.386 |
| 10 | 2 | 1 | 170.8 | 0.274 |
| 10 | 2.5*↓ | 1 | 242.8 | 0.235 |

(* ↓ Precipitation)

**2.3.1.2 Effect of different components.** Miriplatin-loaded micelles with different ratio of lecithin were prepared by thin-film hydration followed by size and PDI measurements. As shown in Table 5, the size of Miriplatin-loaded micelles (PE-PEG$_{2000}$: Miriplatin=10:2) was reduced from 122.2 nm to 95.22 nm and to 75.77 nm with lecithin (PE-PEG$_{2000}$: lecithin=10:0. 5 and 10:1). The chemical structure of lecithin contains a glycerol backbone esterified with two fatty acids and a phosphate group, so it has great emulsifying property and is widely applied as a surfactant for nano formulations. In our studies, lecithin was a surfactant component and helped forming small Miriplatin-loaded micelles. Without lecithin, Miriplatin-loaded micelle (PE-

$PEG_{2000}$: Miriplatin=10:2.5) preparations gave white precipitation, which indicated Miriplatin exceeded the capacity of drug loading (around PE-$PEG_{2000}$: Miriplatin=10:2). However, with lecithin (PE-$PEG_{2000}$: lecithin=10:4), the solution of Miriplatin-loaded micelle (PE-$PEG_{2000}$: Miriplatin=10:5) was still clear and homogeneous (PDI= 0.128) without precipitation. In addition, the size of Miriplatin-loaded micelle (PE-$PEG_{2000}$: Miriplatin=10:5) was 121.1 nm, which was even smaller than Miriplatin-loaded micelle (PE-$PEG_{2000}$: Miriplatin=10: 2.5, 270.8 nm in diameter). Therefore, lecithin can significantly expand the drug loading capacity of Miriplatin-loaded micelles.

Table 5

*Size and PDI of Miriplatin-loaded Micelles with Different Components*

| Compositions (molar ratios) | | | Size (nm) | PDI |
|---|---|---|---|---|
| PE-$PEG_{2000}$ | Miriplatin | Lecithin | | |
| 10 | 2 | - | 122.2 | 0.180 |
| 10 | 2.5* ↓ | - | 270.8 | 0.342 |
| 10 | 2 | 0.5 | 95.22 | 0.313 |
| 10 | 2 | 1 | 75.77 | 0.308 |
| 10 | 5 | 4 | 121.1 | 0.128 |

(* ↓ Precipitation)

**2.3.1.3 Effect of different storage conditions.** Miriplatin-loaded micelles were stored at room temperature for 0 day (fresh prepared), 12 days and 16 days. The size and PDI were measured and are listed in Table 6. When stored at 4℃, there was lots of precipitation appearing. Therefore, Miriplatin-loaded formulations cannot be stored at 4℃. However, at room temperature, the size and PDI of the micelles loaded with Miriplatin after 12 and 16 days were similar to those of freshly prepared ones. In addition, no further precipitation was observed.

This indicates that Miriplatin-loaded formulations can be stored more stably at room temperature. In addition, some Miriplatin-loaded micelles were lyophilized for long-term storage. After reconstitution, they had similar sizes and PDI to freshly prepared ones without precipitation.

Table 6

*Size and PDI of Miriplatin-loaded Micelles at Room Temperature with Different Storage Time*

| Compositions (molar ratios) | | | 0 days | | After 12 days | | 16 days | | Lyophilize | |
|---|---|---|---|---|---|---|---|---|---|---|
| PE-$PEG_{2000}$ | Miri | PTX | Size (nm) | PDI | Size (nm) | PDI | Size (nm) | PDI | Size (nm) | PDI |
| 10 | 1.5 | - | 11.66 | 0.676 | 12.61 | 0.529 | 11.43 | 0.682 | - | - |
| 10 | 2 | - | 12.39 | 0.624 | 12.33 | 0.572 | 13.50 | 0.533 | - | - |
| 10 | 2.5 | - | 270.8 | 0.342 | 302.5 | 0.204 | 281.8 | 0.329 | - | - |
| 10 | 1 | 1 | 208.3 | 0.187 | 204.5 | 0.108 | 205.3 | 0.100 | - | - |
| 10 | 1.5 | 1 | 11.84 | 0.659 | 11.86 | 0.711 | 12.12 | 0.636 | - | - |
| 10 | 2 | 1 | 80.73 | 0.386 | 79.57 | 0.348 | 56.03 | 0.374 | 95.69 | 0. 331 |
| 10 | 2.5* ↓ | 1 | 242.8 | 0.235 | 200.2 | 0.249 | 269.2 | 0.314 | - | - |

(* ↓ Precipitation, Miri: Miriplatin PTX: Paclitaxel)

### 2.3.2 Sizes and PDI of Liposomes Loaded with Different Ratios of Miriplatin

Liposomes with different ratios of drug input were prepared and their sizes and PDI values are shown in Table 7. The lipid compositions of these liposomes were the same (DPPC: cholesterol: PE-$PEG_{2000}$= 15:4:1). As shown in Table 7, the size and PDI of the liposomes with Miriplatin were larger than those without Miriplatin. As the molar ratio of Miriplatin input to PE-$PEG_{2000}$ increased from 2:1 to 8:1, the liposome size decreased. The PDI values of the liposomes with or without Miriplatin were all below 0.25, which indicated that those

formulations were homogeneous. As mentioned earlier, Miriplatin with two 14-Carbon hydrocarbon chains can be considered as both an anticancer payload drug and a lipid component of the formulations. When the ratios of Miriplatin input increased to appropriate level, Miriplatin would be well compacted with other lipids to form denser formulations of smaller sizes without precipitation.

Table 7

*Size and PDI of Liposomes Loaded with Miriplatin at Different Molar Ratios*

| Compositions (molar ratios) | | | | Size (nm) | PDI |
|---|---|---|---|---|---|
| DPPC | Cholesterol | PE-PEG$_{2000}$ | Miriplatin | | |
| 15 | 4 | 1 | - | 187.4 | 0.141 |
| 15 | 4 | 1 | 2 | 225.7 | 0.208 |
| 15 | 4 | 1 | 4 | 187.6 | 0.108 |
| 15 | 4 | 1 | 8 | 163.8 | 0.193 |

### 2.3.3 Size and PDI of Miriplatin-loaded Solid Lipid Nanoparticles (SLNs)

**2.3.3.1 Effect of different ratios of drug input.** SLNs with different molar ratios of Miriplatin were prepared by thin-film hydration. Their size and PDI were measured, and the resultant values are listed in Table 8. In most cases, SLNs with a higher ratio of Miriplatin input had bigger sizes. Furthermore, when the molar ratios of Miriplatin to PE-PEG$_{2000}$ reached 8:4 or higher, white precipitation was observed, which indicated that the SLN compositions (TP or TM: PE-PEG$_{2000}$=36:4) were not ideal for SLN loaded with Miriplatin (when Miriplatin: PE-PEG$_{2000}$ =8:4 or higher)

Table 8

*Size and PDI of SLNs Loaded with Miriplatin at Different Molar Ratios*

| Compositions (molar ratios) | | | | Size (nm) | PDI |
|---|---|---|---|---|---|
| TP | TM | PE-PEG$_{2000}$ | Miriplatin | | |
| 36 | - | 4 | 4 | 106.10 | 0.343 |
| 36 | - | 4 | 8* ↓ | 86.88 | 0.261 |
| 36 | - | 4 | 12* ↓ | 162.30 | 0.275 |
| - | 36 | 4 | 4 | 57.34 | 0.656 |
| - | 36 | 4 | 8* ↓ | 91.45 | 0.241 |
| - | 36 | 4 | 12* ↓ | 150.70 | 0.307 |

(TP: tripalmitin, TM: trimyristin, * ↓ Precipitation)

**2.3.3.2 Effect of Different Ratios of Lipid Compositions.** The effect of lipid compositions (TP or TM and PE-PEG$_{2000}$) on the sizes of their Miriplatin-loaded solid lipid nanoparticles prepared by thin-film hydration method are shown in Table 9. The size of SLNs loaded with 10% Miriplatin ranged from180 nm to 20 nm in diameter. Most of their PDI values were below 0. 6. As the molar ratio of PE-PEG$_{2000}$ to TP or TM increased (from 39:1 to 24:16), the size of the SLNs decreased. As a reference, micelles, whose lipid composition could be regarded as no solid lipid (TP or TM) and all PE-PEG$_{2000}$, also can be fit into this trend. Moreover, for the same molar ratio of solid lipids and PE-PEG$_{2000}$, most sizes of SLNs consisting of solid lipid TP were slightly bigger than the SLNs consisting of solid lipid TM.

Table 9

*Size and PDI of Miriplatin-Loaded SLNs with Different Ratios of Lipid Compositions*

| Compositions (molar ratios) | | | | Size (nm) | PDI |
|---|---|---|---|---|---|
| TP | TM | PE-PEG$_{2000}$ | Miriplatin | | |
| 39 | - | 1 | 4 | 177.20 | 0.403 |
| - | 39 | 1 | 4 | 141.30 | 0.191 |
| 38 | - | 2 | 4 | 195.00 | 0.512 |
| - | 38 | 2 | 4 | 121.30 | 0.262 |
| 36 | - | 4 | 4 | 106.10 | 0.343 |
| - | 36 | 4 | 4 | 57.34 | 0.856 |
| 32 | - | 8 | 4 | 79.31 | 0.413 |
| - | 32 | 8 | 4 | 131.40 | 0.217 |
| 24 | - | 16 | 4 | 22.81 | 0.846 |
| - | 24 | 16 | 4 | 18.81 | 0.500 |
| Micelle: - | Micelle: - | 40 | 4 | 11.24 | 0.579 |

(TP: tripalmitin, TM: trimyristin)

**2.3.3.3 Effect of other components (Tween 20, Tween 80, Lecithin and Cholesterol).**

As shown in Table 10, incorporation of 1.5% (v/v) Tween 20 into the blank TP SLN (TP: PE-PEG$_{2000}$=38:2) significantly reduced the size from 141.3 nm to 9.47 nm. The size of blank TM SLN containing 1.5% (v/v) Tween20 also has a similar trend. Because the typical size range of solid lipid nanoparticles is 50-500 nm [63], the blank nano formulations (TP/TM: PE-PEG$_{2000}$=38:2) containing 1.5%(v/v) Tween20 were probably micelles rather than SLNs. Therefore, such formulations were not subjected to further studies. In addition, incorporation of 1% (v/v) Tween80 increased the size of TP SLNs from less than 200 nm to more than 250 nm. However, TM SLNs had an opposite trend. The sizes of TM SLNs containing 1% (v/v) Tween80 were smaller than those without Tween 80. This is probably because the head group

and chain length of Tween 80 fitted better with solid lipid TM. However, Tween 20 and Tween 80 were viscous liquids at room temperature, and the amount of addition was difficult to control, which prevented further research and application on such formulations.

Table 10

*Size and PDI of Miriplatin-loaded SLNs with Tween 20 or Tween 80*

| Compositions (molar ratios) | | | | Other Components | | Size (nm) | PDI |
|---|---|---|---|---|---|---|---|
| TP | TM | PE-PEG$_{2000}$ | Miriplatin | Tween20 | Tween80 | | |
| 39 | - | 1 | - | - | - | 141.30 | 0.737 |
| 39 | - | 1 | - | 1.5% (v/v) | - | 9.47 | 0.792 |
| 39 | - | 1 | 4 | - | - | 195.00 | 0.512 |
| 39 | - | 1 | 4 | - | 1% (v/v) | 260.40 | 0.315 |
| 38 | - | 2 | 4 | - | - | 106.10 | 0.343 |
| 38 | - | 2 | 4 | - | 1% (v/v) | 296.10 | 0.302 |
| - | 39 | 1 | - | - | - | 101.60 | 0.349 |
| - | 39 | 1 | - | 1.5% (v/v) | - | 8.91 | 0.579 |
| - | 39 | 1 | 4 | - | - | 121.30 | 0.262 |
| - | 39 | 1 | 4 | - | 1% (v/v) | 108.50 | 0.317 |
| - | 38 | 2 | 4 | - | - | 117.52 | 0.326 |
| - | 38 | 2 | 4 | - | 1% (v/v) | 107.50 | 0.348 |

(TP: tripalmitin, TM: trimyristin)

As shown in Table 11, the sizes of Miriplatin-loaded SLNs including cholesterol (cholesterol: PE-PEG$_{2000}$= 4:16) were smaller than those without cholesterol. As a component of lipid bilayer structure, cholesterol can occupy the cavities between fatty acid chains to inhibit the movement of hydrocarbon chains and to improve the stability of lipid-based nanoparticles.

Table 11

*Size and PDI of Miriplatin-loaded SLNs with Cholesterol*

| Compositions (molar ratios) | | | | | | Size (nm) | PDI |
|---|---|---|---|---|---|---|---|
| TP | TM | PE-PEG$_{2000}$ | Miriplatin | PTX | Cholesterol | | |
| 24 | - | 16 | 8 | - | - | 141.30 | 0.275 |
| 20 | - | 16 | 8 | - | 4 | 113.40 | 0.423 |
| - | 24 | 16 | 8 | - | - | 140.10 | 0.351 |
| - | 20 | 16 | 8 | - | 4 | 90.19 | 0.677 |
| 24 | - | 16 | 8 | 4 | - | 117.70 | 0.512 |
| 20 | - | 16 | 8 | 4 | 4 | 94.62 | 0.410 |
| - | 24 | 16 | 8 | 4 | - | 116.40 | 0.859 |
| - | 20 | 16 | 8 | 4 | 4 | 95.81 | 1.000 |

(TP: tripalmitin, TM: trimyristin, PTX: Paclitaxel)

The result of size and PDI of Miriplatin-loaded SLNs with lecithin are shown in Table 12. As a surfactant component for lipidic formulations, lecithin (lecithin: PE-PEG$_{2000}$= 2:16) increased the sizes of TP- and TM-based SLNs that are loaded with Miriplatin, however, when the molar ratios of lecithin to PE-PEG$_{2000}$ increased from 2:16 to 4:16, the sizes of SLNs decreased. This is probably because the compositions of SLNs were complex, when the molar ratios of lecithin to PE-PEG$_{2000}$ came to 4:16, lecithin reached a balanced molar ratio with lipid components and input drug.

Table 12

*Size and PDI of Miriplatin-loaded SLNs with Lecithin*

| Compositions (molar ratios) | | | | | Size (nm) | PDI |
|---|---|---|---|---|---|---|
| TP | TM | PE-PEG$_{2000}$ | Miriplatin | Lecithin | | |
| 24 | - | 16 | 8 | - | 141. 30 | 0. 275 |

(Table 12 Continued)

| | | | | | | |
|---|---|---|---|---|---|---|
| 24 | - | 16 | 8 | 2 | 205. 4 | 0. 307 |
| 24 | - | 16 | 8 | 4 | 80. 44 | 0. 290 |
| - | 24 | 16 | 8 | - | 116. 40 | 0. 859 |
| - | 24 | 16 | 8 | 2 | 279 | 0. 562 |
| - | 24 | 16 | 8 | 4 | 99. 29 | 0. 489 |

(TP: tripalmitin, TM: trimyristin)

**2.3.3.4 Effect of different molar ratios of solid lipids.** According to the results shown in Table 11, for the same ratio of solid lipids and PE-$PEG_{2000}$, most sizes of SLNs consisting of the solid lipid TP were slightly bigger than the SLNs consisting of the solid lipid TM. In addition, we attempted to develop SLNs with both TP and TM. As shown in Table 13, the sizes of SLNs containing both TP and TM were much larger than SLNs with only TP or TM.

Table 13

*Size and PDI of Miriplatin-loaded SLNs with TP and TM*

| Compositions (molar ratios) | | | | | Size (nm) | PDI |
|---|---|---|---|---|---|---|
| TP | TM | PE-$PEG_{2000}$ | Miriplatin | Paclitaxel | | |
| 18 | 18 | 4 | 8 | 4 | 233.4 | 0.272 |
| 12 | 12 | 16 | 8 | 4 | 286.9 | 0.196 |

(TP: tripalmitin, TM: trimyristin)

## 2.4 Summary

Lipid-based nanoparticles (micelles, liposomes, solid lipid nanoparticles) with Miriplatin as the payload drug were successfully developed by the thin-film hydration method. We investigated formulations with many variations in lipid composition, including different lipid

components, different lipid molar ratios, different drug input molar ratios, different solid lipid molar ratios, and different ratios of additional ingredients such as Tween 20, Tween 80, lecithin, and cholesterol. Higher molar ratios of the pegylated lipid (PE-$PEG_{2000}$) in lipid compositions can decrease the size of formulations. Among three types of lipid-based nanoparticles, most of the micelles had much smaller sizes (~ 10 nm), while most liposomes and SLNs were much larger (80 nm to 200 nm). In future studies, the lipid compositions could be further optimized to improve the homogeneity and reproducibility of Miriplatin-loaded formulations.

# CHAPTER 3: PHYSICOCHEMICAL CHARACTERIZATION OF LIPID-BASED NANOPARTICLES OF MIRIPLATIN

## 3.1 Introduction

### 3.1.1 Solubility of Miriplatin

Miriplatin is a lipophilic platinum derivative containing two C14:0 myristates as a carrier ligand[89, 90]. Clinically, it is a third-generation platinum complex that was developed and approved as a chemotherapeutic drug for hepatocellular carcinoma (HCC) in Japan (Miripla®, Dainippon Sumitomo Pharma, Osaka, Japan) [45, 91]. To date, Miriplatin can only be administered by hepatic artery embolization for interventional treatment of HCC, which greatly limits its clinical application [92, 93]. Miriplatin forms a suspension in an oily lymphographic agent (Lipiodol Ultra-Fluide®, LPD). In iodized oil, the platinum released from the suspension retained in the HCC participates in the anti-cancer effect [45]. The limited application of Miriplatin is mainly due to its extremely low solubility in water (<0.00260 mg/mL) [94]. Miriplatin also has poor solubility in organic solvents that are commonly used in research laboratories, such as methanol, ethanol, acetonitrile, and acetone. So far only chloroform is known to readily dissolve Miriplatin at >1mg/mL. The low solubility of Miriplatin increases the difficulty of characterizing Miriplatin-loaded formulations.

### 3.1.2 Quantification of the Platinum Element

Inductively coupled plasma emission spectroscopy (ICP-OES), is an analytical technique used to detect the composition of chemical elements. It has been commercially available since 1974 [95]. This technology uses the unique photophysical signal of each element to detect the type and relative content of each element in complex samples. ICP-OES is an emission

spectroscopy technology that uses inductively coupled plasma to generate excited atoms and ions that emit electromagnetic radiation at the characteristic wavelength of a specific element, where plasma is a high temperature source of ionization source gas (usually argon). The plasma of ICP-OES is maintained by inductive coupling from a cooling electric coil at a megahertz frequency [95, 96]. In this way, ICP-OES can trace and quantify specific elements in pharmaceutical formulations. The United States Pharmacopoeia (USP) has published guidelines of using ICP-OES to ensure that certain impurities in pharmaceutical products are within legal limits [97]. In recent years, ICP-OES has become the best technique for quantifying impurities in pharmaceuticals. Moreover, it plays an important role in the determination of elements in human blood, urine and other biological matrices [98].

Inductively coupled plasma mass spectrometry (ICP-MS), which is a technique closely related to ICP-OES, was also introduced in the USP and the International Conference of Harmonization (ICH Q3D) guidelines for measurement of chemical elements at trace levels in biological fluids [16, 99]. Due to differences in the detection of metal elements, the detection limit of ICP-MS can be extended to one part per trillion (ppt), while the detection limit of ICP-OES is one part per billion (ppb). The detection limit of ICP-MS is usually 3 orders of magnitude lower than that of ICP-OES, mainly because there is no basic source of continuum background in ICP-MS [95]. The limit of detection of ICP-MS can be extended to one part per trillion (ppt) whereas the limit of ICP-OES is one part per billion (ppb) [74]. However, compared with ICP-OES, the method development of ICP-MS is more difficult and costly [74].

In this study, ICP-OES and ICP-MS methods were developed in order to quantify the recovery rate of platinum in Miriplatin-loaded formulations, which is defined as the percentage of the total platinum input that is detected by ICP-OES or ICP-MS.

### 3.1.3 Quantification of Intact Miriplatin

Miriplatin, which contains myristate as a leaving group to improve lipophilicity, is chemically designed as an antitumor agent more suitable for long-term trans arterial chemoembolization [100]. The anti-tumor platinum complex undergoes a leaving group exchange prior to the reaction with DNA in tumors. However, in physiological environments biological nucleophiles including chlorides, sulfur-containing amino acids, and glutathione, can displace the leaving group of Miriplatin and lead to inactivation of the drug at the concentration where it showed anticancer activity in culture medium or serum [6, 101, 102]. Nevertheless, platinum complexes containing lipophilic leaving groups are expected to dissolve or easily suspend in LPD; after hepatic artery administration, they are expected to gradually release and exert activity in liver, where the tumor resides, thus reducing systemic circulation and toxicity [6]. Miriplatin and its metabolites in physiological surroundings were analyzed by high performance liquid chromatography (HPLC) [6, 103]. In addition, for Miriplatin-loaded formulations, Xia's lab established a quantification method for Miriplatin and Miriplatin-loaded liposomes by HPLC [104].

In this study, a quantification method of intact Miriplatin inside Miriplatin-loaded formulations was developed, using HPLC.

### 3.1.4 Morphology of Miriplatin-loaded Formulations

Transmission electron microscopy (TEM) is a popular technology for nanoscale structural characterization. According to the imaging, diffraction and microanalysis information gained from TEM, the characteristics and behavior of nanostructured materials can be determined by TEM [105]. The particle size distribution, particle size uniformity, lattice type, and morphological information can all be obtained by TEM, which makes it a powerful and

essential technique for characterization of the nanomaterials such as nanoparticles [106]. The principle of TEM is to image samples by detecting the trajectory change of an electron beam as it passes through an ultra-thin sample. The electron beam is focused by strong magnetic fields and the electrons are found in a spiral trajectory. An image is formed and magnified from the electrons transmitted through the specimen, and then is magnified. and the imaged is focused on an objective lens, and the image appears on an imaging screen [106]. The classic processing of specimens observed in a TEM needs fixation, dehydration, preparation of thin sections, and staining [107]. To visualize the structure and size, negative staining is more efficient than the positive staining [108]. During TEM sample preparations, it is necessary to use a grid to make the sample uniformly thin and thus to allow the beam of electrons to penetrate [109].

The objective of this chapter is to characterize the physiochemical properties and morphology of Miriplatin-loaded formulations. In this study, the Miriplatin-loaded formulations were negatively stained by uranyl acetate before imaging by TEM. The morphology and particles sizes of lipid-based nanoparticles of different compositions were compared.

## 3.2 Materials and Methods

### 3.2.1 Materials

Miriplatin was purchased from MedChem Express LLC (NJ, US). Paclitaxel was purchased from LC Laboratory (MA, US). All other organic solvent and chemicals were purchased from Sigma Aldrich, Fisher Scientific or VWR. Two-hundred mesh continuous carbon-coated copper grids were purchased from TED PELLA (CA, US).

### 3.2.2 Quantification of Platinum Recovery from Miriplatin-Loaded Formulations by ICP-OES and ICP-MS

To quantify the platinum recovery for Miriplatin-loaded formulations, different reagents (sulfuric acid, nitric acid, and aqua regia) were used for sample digestion in preliminary studies. For the digestion by sulfuric acid, aliquots (50 μL for each sample) of formulations were placed into Pyrex tubes and diluted by 1 mL 10 N sulfuric acid. The samples were then heated in a solid anodized aluminum heating block in the fume hood at 200-210 ℃ for 60 min. The tubes were removed from heating and cooled at room temperature for 10 min. Then an aliquot (0.25 mL) of 10% hydrogen peroxide was added to each tube. All tubes were heated at 190-200 ℃ for 10 min and then cooled at room temperature for 10 min. For sample digestion by nitric acid, aliquots (50 μL each) of formulations were added to tubes and diluted with 3.45 mL 70% concentrated nitric acid. The samples were heated at 90 ℃ for 90 min and then cooled to room temperature. Then an aliquot (500 μL) of each digestion solution was diluted with 6.5 mL deionized water to make the concentration of nitric acid reach 5%, which is suitable for injection into ICP-OES and ICP-MS. In addition, although microwave-assisted aqua regia digestion is widely used for determining platinum element [110, 111], this method was not used in our comprehensive studies because it was much more dangerous than other digestion methods and required high-fold dilutions.

Each sample was measured in triplicate. The concentration of platinum in Miriplatin-loaded formulations was estimated from the calibration curve of the platinum standard solutions. The formula for calculating platinum recovery from Miriplatin-loaded formulation is as follows:

$$Platinum\ recovery\ (\%) = \frac{Platinum\ amount\ detected\ by\ ICP-OES\ or\ ICP-MS}{Platinum\ amount\ input\ in\ miriplatin-loaded\ fomulations} \times 100\%$$

### 3.2.3 Quantification of Intact Miriplatin in Miriplatin-Loaded Formulations by HPLC

Quantification of Miriplatin was performed by high performance liquid chromatography (HPLC) equipped with Waters 2695 separations module coupled to a 2996 photodiode array detector. The stationary phase (Agilent ZORBAX SB-C8, 3.5 μm; 4.6 × 150 mm) was kept at 25 ℃, and the mobile phase (methanol: water = 92:8, v/v) was run at the flow rate of 1 mL/min. Effluent was monitored at wavelength 210 nm. The retention time of intact Miriplatin was about 9.7 min. First, 50 μL Miriplatin-loaded formulation was taken and diluted with 950 μL methanol. Then the sample was centrifuged at 12000 rpm for 10 minutes, and the supernatant was taken for HPLC analysis. An aliquot (20 μL) of each sample was injected into HPLC after preparation. The concentration of intact Miriplatin in Miriplatin-loaded formulations was estimated from the calibration curve of the Miriplatin standard solutions. The formula for calculating intact Miriplatin recovery from Miriplatin-loaded formulations is as follows:

$$Intact\ miriplatin\ recovery\ (\%) = \frac{Intact\ miriplatin\ amount\ detected\ by\ HPLC}{Miriplatin\ amount\ input\ in\ miriplatin-loaded\ fomulations} \times 100\%$$

### 3.2.4 Morphology of Miriplatin-Loaded Formulations by TEM

The morphology of Miriplatin-loaded formulations with different components was imaged on a JEOL-JEM 1230 Electron Microscope (JEOL, Japan). The Miriplatin-loaded formulations were negatively stained by uranyl acetate. In order to increase hydrophilicity, 200 mesh carbon-coated copper grids were exposed to glow discharge before usage. An aliquot (5 μL) of formulations was added onto the grid and air-dried for 60 seconds. The excess liquid on the grid was blotted with filter paper to form a thin section, which was then quickly stained with 2% uranyl acetate and blotted dry with filter paper. The grid was then transferred to the electron

microscope for imaging. The digital images of formulations by TEM were analyzed with TIETZ imaging software (EMMENU4).

## 3.3 Results and Discussion

### 3.3.1 Quantification of Platinum Recovery from Miriplatin-Loaded Formulations by ICP-OES

#### 3.3.1.1 Comparison of platinum recovery from different Miriplatin-loaded formulations.

The results of platinum recovery rate in formulations were similar between nitric acid digestion and sulfuric acid digestion methods. Based on our preliminary data, nitric acid digestion was selected as the general digestion method for ICP-OES and ICP-MS to quantify the platinum element. The platinum recovery from Miriplatin-loaded micelles and solid lipid nanoparticles (SLNs) by ICP-OES are shown in Table 14, Table 15, and Table 16. All the formulations were digested by 70% nitric acid at 90 ℃ for 90 min. As negative control, the platinum recovery from blank micelles and SLNs (no drug loading) was close to zero. For Miriplatin-loaded formulations, all the platinum recovery rates were above 50%. Specifically, as shown in Table 14, the platinum recovery of Miriplatin-loaded micelle was close to 100% (110.54%), which indicated that almost all of the Miriplatin input during preparation was still in the formulation solution. Selected SLNs (such as SLN-9,10,11,12,15,16) also had high platinum recovery that was similar to micelles. While other SLNs had much lower platinum recovery (from 13.55% to 72.23%) than micelles.

The results of platinum recovery cannot be simply considered as the encapsulation efficiency of Miriplatin-loaded formulations because the ICP-OES (also ICP-MS) traced all forms of the platinum element. As we mentioned in the introduction, Miriplatin may lose one or two myristate chains during the preparation. Therefore, other forms of platinum molecules

(Miriplatin degradation products) would still be detected by ICP-OES. Moreover, because of the limited volume of the formulations (less than 300μL), we could not separate unloaded free Miriplatin from the nano- formulations. Therefore, undissolved Miriplatin could be also digested and detected. In this way, the actual encapsulation efficiency might be lower than the platinum recovery by ICP-OES measurements.

Table 14

*Platinum Recovery from Miriplatin-loaded Micelles by ICP-OES*

| Formulations | Compositions (molar ratios) | | Platinum Recovery (%) |
|---|---|---|---|
| | PE-PEG$_{2000}$ | Miriplatin | |
| Micelle-1 | 10 | - | 0.25 |
| Micelle-2 | 10 | 2 | 110.54 |

(PE-PEG$_{2000}$: 1,2-distearoyl-*sn*-glycero-3-phosphoethanolamine-N- [methoxy (polyethylene glycol)-2000] (ammonium salt))

Table 15

*Platinum Recovery from Miriplatin-loaded SLNs with Different Molar Ratios of Solid Lipid (TP/TM) and PE-PEG$_{2000}$ by ICP-OES*

| Formulations | Compositions (molar ratios) | | | | Platinum Recovery (%) |
|---|---|---|---|---|---|
| | TP | TM | PE-PEG$_{2000}$ | Miriplatin | |
| SLN-1 | 39 | - | 1 | - | 0.00 |
| SLN-2 | - | 39 | 1 | - | 0.00 |
| SLN-3 | 39 | - | 1 | 4 | 13.55 |
| SLN-4 | - | 39 | 1 | 4 | 17.28 |
| SLN-5 | 38 | - | 2 | - | 0.61 |
| SLN-6 | - | 38 | 2 | - | 0.085 |
| SLN-7 | 38 | - | 2 | 4 | 61.21 |
| SLN-8 | - | 38 | 2 | 4 | 34.40 |

(Table 15 Continued)

| | | | | | |
|---|---|---|---|---|---|
| SLN-9 | 36 | - | 4 | 4 | 128.81 |
| SLN-10 | - | 36 | 4 | 4 | 94.78 |
| SLN-11 | 32 | - | 8 | 4 | 99.01 |
| SLN-12 | - | 32 | 8 | 4 | 101.73 |

(TM: trimyristin, TP: tripalmitin, PE-PEG$_{2000}$: 1,2-distearoyl-*sn*-glycero-3-phosphoethanolamine-N- [methoxy (polyethylene glycol)-2000] (ammonium salt))

Table 16

*Platinum Recovery from Miriplatin-loaded SLNs with Cholesterol by ICP-OES*

| Formulations | Compositions (molar ratios) | | | | | | Platinum Recovery (%) |
|---|---|---|---|---|---|---|---|
| | TP | TM | PE-PEG$_{2000}$ | Miriplatin | PTX | Cholesterol | |
| SLN-13 | 24 | - | 16 | - | - | - | 2.53 |
| SLN-14 | - | 24 | 16 | - | - | - | 0.66 |
| SLN-15 | 24 | - | 16 | 8 | - | - | 99.66 |
| SLN-16 | - | 24 | 16 | 8 | - | - | 100.98 |
| SLN-17 | 24 | - | 16 | 8 | 4 | - | 72.23 |
| SLN-18 | - | 24 | 16 | 8 | 4 | - | 62.75 |
| SLN-19 | 20 | - | 16 | 8 | - | 4 | 66.63 |
| SLN-20 | - | 20 | 16 | 8 | - | 4 | 72.21 |
| SLN-21 | 20 | - | 16 | 8 | 4 | 4 | 52.76 |
| SLN-22 | - | 20 | 16 | 8 | 4 | 4 | 62.59 |

(TM: trimyristin, TP: tripalmitin, PTX: Paclitaxel, PE-PEG$_{2000}$: 1,2-distearoyl-*sn*-glycero-3-phosphoethanolamine-N- [methoxy (polyethylene glycol)-2000] (ammonium salt))

**3.3.1.2 Platinum recovery from Miriplatin-loaded SLNs with different molar ratios of solid lipid (TP/TM) and PE-PEG$_{2000}$.** The platinum recovery from Miriplatin-loaded SLNs with different molar ratios of components were detected by ICP-OES. As shown in Table 15, as

the molar ratio of PE-$PEG_{2000}$ to TP increased from 1:39 to 8:32, the platinum recovery increased from 13.55% to 99.01%. Similarly, as the molar ratio of PE-$PEG_{2000}$ to TM increased, the platinum recovery from SLNs with TM increased (from 17.28% to 101.7%). This indicates that PE-$PEG_{2000}$ as a lipid component facilitated the loading of Miriplatin into the formulations.

**3.3.1.3 Platinum recovery from SLNs loaded with Miriplatin and Paclitaxel**. The platinum recovery from SLNs co-formulated with Paclitaxel was compared to SLNs without Paclitaxel (Table 16). For Miriplatin-loaded SLNs with TP, SLNs with Miriplatin and Paclitaxel had lower platinum recovery (72.23%) than SLNs loaded only with Miriplatin (99.66%). Miriplatin-loaded SLNs with TM had similar trend in that the coformulation of Paclitaxel decreased the platinum recovery from 100.98% to 62.75%. This is probably due to the limitation of drug loading capacity of SLNs. When cholesterol was included as an additional lipid component, the Miriplatin-loaded SLNs showed similar platinum recoveries with or without Paclitaxel.

### 3.3.2 Quantification of Platinum Recovery from Miriplatin-Loaded Formulations by ICP-MS

The composition and platinum recovery of Miriplatin-loaded micelles and solid lipid nanoparticles (SLNs) by ICP-MS are shown in Table 17. The formulations were digested by 70% nitric acid at 90 ℃ for 90 min. The platinum recovery rates of all Miriplatin-loaded formulations are around 100%. Compared to the platinum recovery rates of SLN-24 and SLN-15 (in Table 16, by ICP-OES), they had the similar results with same molar ratios of components. Furthermore, Miriplatin-loaded SLNs with Paclitaxel (SLN-25) had lower platinum recovery (91.76%) than SLNs loaded only with Miriplatin (105%). Compared to SLNs, Miriplatin-loaded micelles

(Micelle-4 and 5) showed the same trend of decreasing platinum recovery rate from 165.38% to 115.98% when Paclitaxel is also loaded.

The platinum recovery rates of some Miriplatin-loaded formulations appear to be much higher than 100%, such as Micelle-4 (165.38%) (Table 17). A probable reason is that during the preparation, the temperature of hydration was high (about 78℃) and the volume of formulation was very limited (less than 300 μl), so the formulation solution might be partially evaporated. Although we refilled DI water and tried to restore the original volume, some samples might be concentrated. Another possible reason is that some platinum might be carried over from one sample to another during detection. In this batch, the micelle without Miriplatin (Micelle-3) was analyzed after Miriplatin-loaded SLNs (SLN-25), and the platinum recovery of Micelle-3 was 12.88%, which was higher than 0%. Platinum carryover might also influence the results of Micelle-4 and 5.

Table 17

*Platinum Recovery from Miriplatin-loaded Formulations by ICP-MS*

| Formulations | Compositions (molar ratios) | | | | Platinum Recovery (%) |
|---|---|---|---|---|---|
| | TP | PE-PEG$_{2000}$ | Miriplatin | PTX | |
| SLN-23 | 24 | 16 | - | - | 2.25 |
| SLN-24 | 24 | 16 | 8 | - | 105.54 |
| SLN-25 | 24 | 16 | 8 | 4 | 91.76 |
| Micelle-3 | - | 40 | - | - | 12.88 |
| Micelle-4 | - | 40 | 8 | - | 165.38 |
| Micelle-5 | - | 40 | 8 | 4 | 115.98 |

(TP: tripalmitin, PTX: Paclitaxel, PE-PEG$_{2000}$: 1,2-distearoyl-*sn*-glycero-3-phosphoethanolamine-N- [methoxy (polyethylene glycol)-2000] (ammonium salt))

### 3.3.3 Quantification of Intact Miriplatin Recovery from Miriplatin-Loaded Formulations by HPLC

As shown in Table 18, the recovery of intact Miriplatin from Miriplatin-loaded micelles was around 100% per HPLC, while Miriplatin-loaded SLNs had much lower intact Miriplatin recovery (about 30%). This is probably because some Miriplatin lost 14-carbon chains during the preparation of Miriplatin-loaded SLNs while higher molar ratio of PE-$PEG_{2000}$ in the micelles might have better protected Miriplatin from degradation. In addition, Miriplatin-loaded SLNs with TM has lower intact Miriplatin recovery (about 30%) than SLNs with TP (about 40%).

Table 18
*Recovery of Intact Miriplatin from Miriplatin-loaded Formulations*

| Formulations | Compositions (molar ratios) | | | | | Intact Miriplatin Recovery (%) |
|---|---|---|---|---|---|---|
| | TP | TM | PE-$PEG_{2000}$ | Miriplatin | PTX | |
| SLN-1 | 24 | - | 16 | 8 | - | 39.60 |
| SLN-2 | 24 | - | 16 | 8 | 4 | 43.76 |
| SLN-3 | - | 24 | 16 | 8 | - | 31.03 |
| SLN-4 | - | 24 | 16 | 8 | 4 | 24.70 |
| Micelle-1 | - | - | 40 | 8 | - | 107.10 |
| Micelle-2 | - | - | 40 | 8 | 4 | 115.06 |

(TM: trimyristin, TP: tripalmitin, PTX: Paclitaxel, PE-$PEG_{2000}$: 1,2-distearoyl-*sn*-glycero-3-phosphoethanolamine-N- [methoxy (polyethylene glycol)-2000])

### 3.3.4 Morphology of Miriplatin-Loaded Formulations by TEM Imaging

**3.3.4.1 Morphology of Miriplatin-loaded micelles.** As shown in Figures 8, and Figure 9, micelles loaded with only Miriplatin, and micelles loaded with both Miriplatin, and Paclitaxel appeared as ultra-small white dots by TEM imaging. The samples showed small, homogeneous

white dots around 10 nm, which was consistent with the results from the Zetasizer. There was no significant difference between these micelles of different drug input.

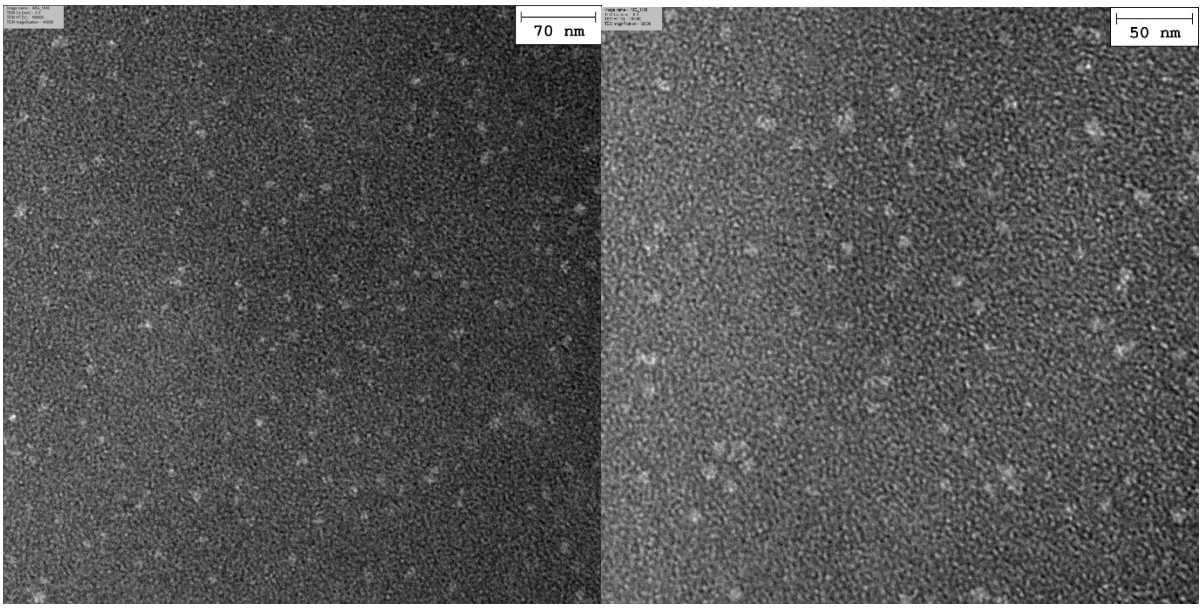


*Figure 8.* TEM images of micelles loaded with Miriplatin as the only cargo drug (PE-$PEG_{2000}$: Miriplatin (molar ratios) =10:2).

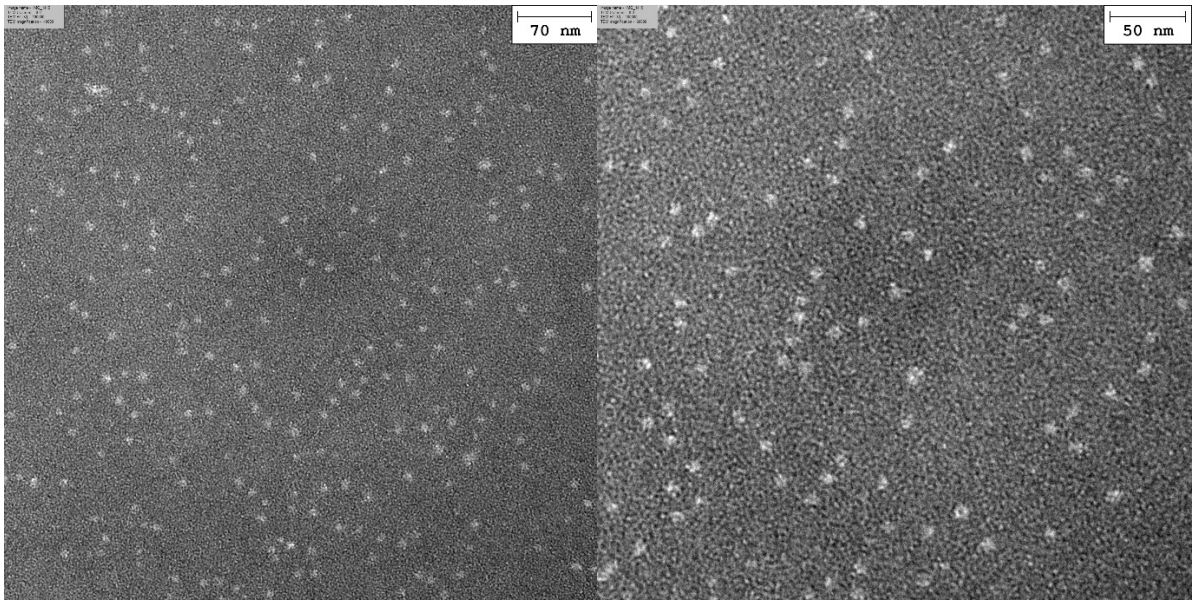


*Figure 9.* TEM images of micelles loaded with Miriplatin and Paclitaxel as payload drugs (PE-$PEG_{2000}$: Miriplatin: Paclitaxel (molar ratios) =10:2:1).

**3.3.4.2 Morphology of Miriplatin-loaded SLNs.** Figures 10, 11, 12, and 13 show the TEM images of SLNs either loaded with only Miriplatin, or with both Miriplatin and Paclitaxel. Almost all TEM images showed a mixture of spherical and rod structures. Compared to the SLNs with TP, SLNs with TM had more rod structures. Prior studies suggest that the shape (aspect ratio, AR) of lipid molecule would impact the shape of their nanoparticles [112]: when the size of the lipid head group is similar to that of the lipid tail (AR is ~1), the lipid molecules would form spheres; when the lipid tail is larger than the lipid head group (AR> 2), they would form more rods [112]. However, the TP SLNs (TP: PE-PEG2000: Miriplatin: Paclitaxel (molar ratios) =24:16:8:4) in our studies showed mostly round-shape spheroids. This might be because that TP (containing 16-carbon chains) could better help PE-PEG2000 (containing 18-carbon chains) and Miriplatin (containing 14-carbon chains) to mix together to form around particles. All round SLNs were about 120 nm in diameter, which was consistent with the results from the Zetasizer.

The ultra-small white dots observed in the TEM images of SLNs might be micelles. The preparation methods of micelles and SLNs were the same (thin-film hydration). But micelles contained simpler composition and much higher molar ratios of PE-PEG2000. Therefore, some Miriplatin-loaded micelles and/or blank micelles might be generated together with SLNs from incomplete mixing of the lipids.

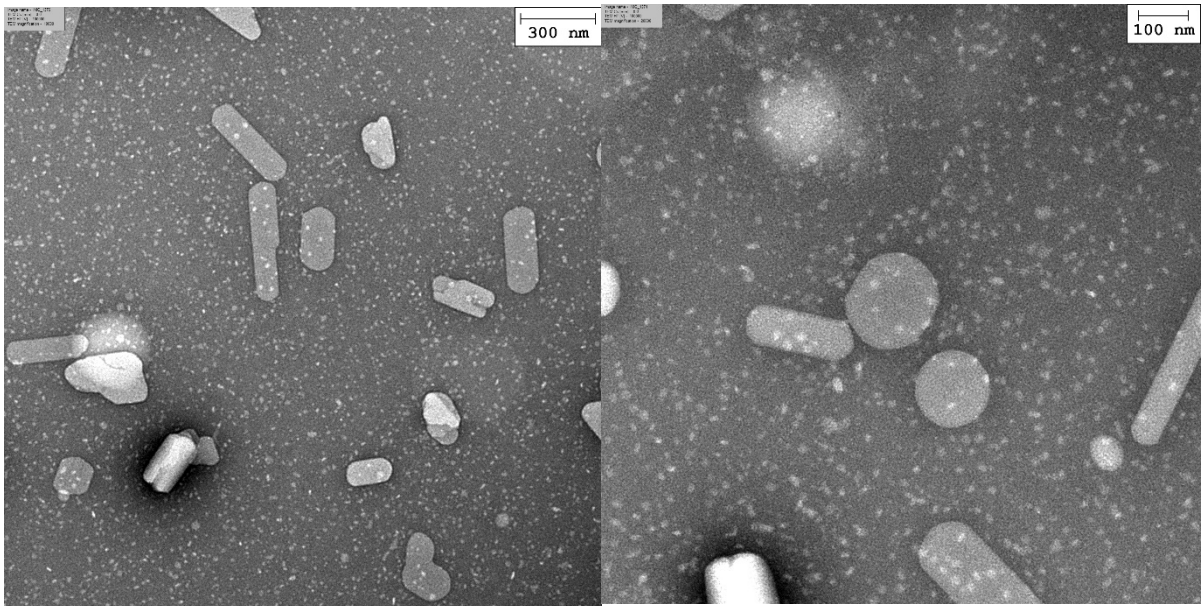


*Figure 10.* TEM images of SLNs consisting of TP: PE-PEG$_{2000}$: Miriplatin (molar ratios) =24:16:8.

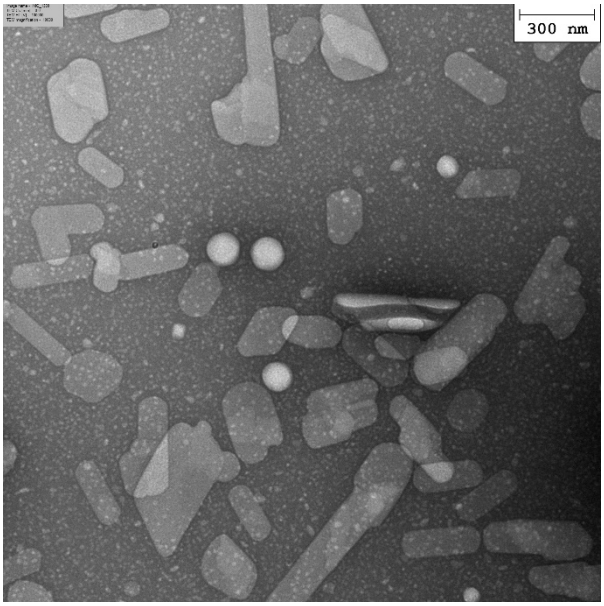


*Figure 11.* TEM image of Miriplatin-loaded SLNs consisting of TM: PE-PEG$_{2000}$: Miriplatin (molar ratios) =24:16:8.

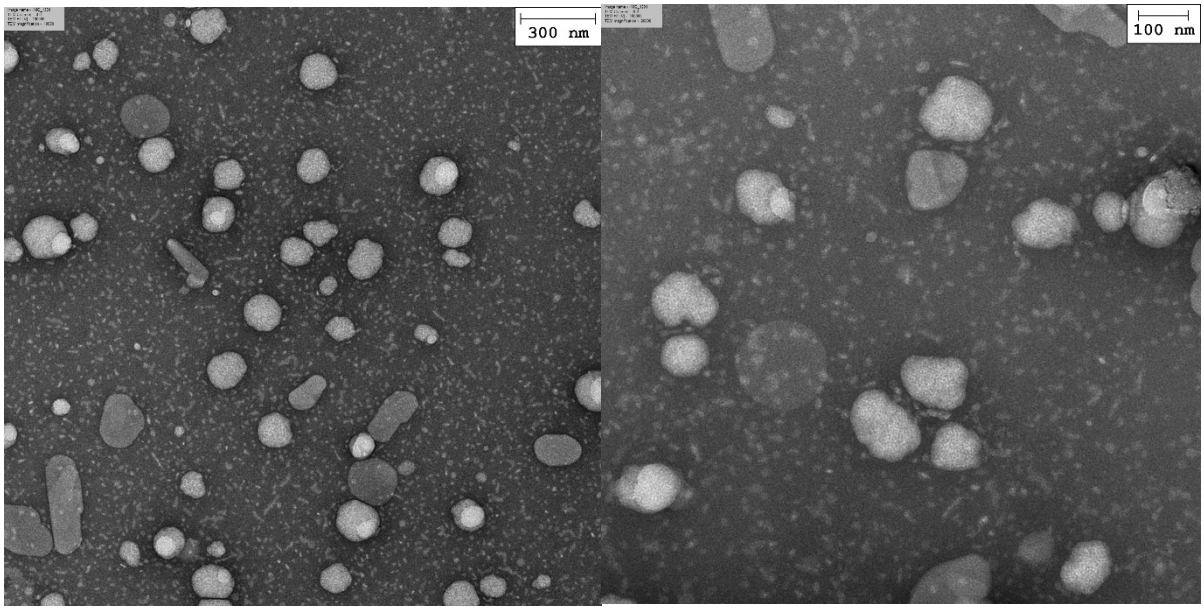


*Figure 12.* TEM images of SLNs consisting of TP: PE-PEG$_{2000}$: Miriplatin: Paclitaxel (molar ratios) =24:16:8:4.

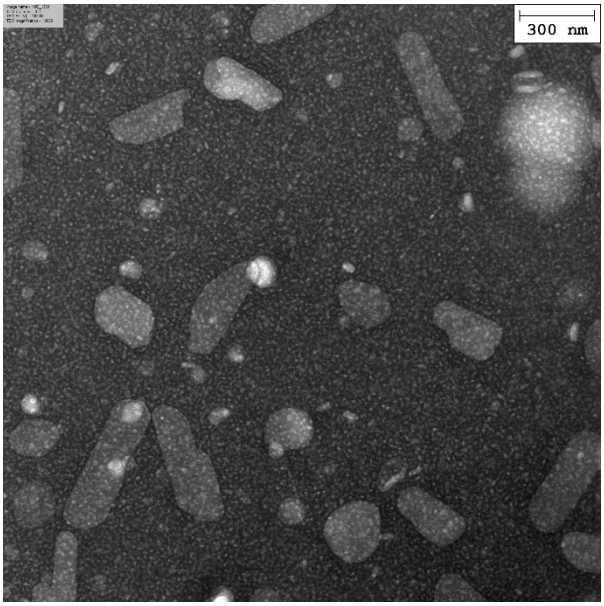


*Figure 13.* TEM image of SLNs consisting of TM: PE-PEG$_{2000}$: Miriplatin: Paclitaxel (molar ratios) =24:16:8:4).

## 3.4 Summary

Both ICP-OES and ICP-MS were used to quantify platinum recovery from Miriplatin-loaded formulations. The results of platinum recovery by ICP-OES and ICP-MS were consistent. Micelles and selected SLNs had high platinum recovery around 100%. The platinum recovery of all Miriplatin-loaded formulations was above 50%. Intact Miriplatin recovery from Miriplatin-loaded formulations was determined by HPLC. Miriplatin-loaded micelles had much higher intact Miriplatin recovery (~100%) than SLNs (~30%).

Miriplatin-loaded formulations were negatively stained with uranyl acetate and then imaged by TEM, which showed the size and morphology of the Miriplatin-loaded formulations. The TEM results were consistent with size and PDI result from the Zetasizer. In the TEM studies, micelles showed a morphology of spherical dots of about 10 nm in diameter while SLNs showed both spherical and rod structures of about 120 nm in diameter.

# CHAPTER 4: EVALUATION OF ANTICANCER ACTIVITY OF MIRIPLATIN-LOADED FORMULATIONS AGAINST 3D MCS

## 4.1 Introduction

In recent decades, various nanotechnology platforms in the field of medical biology including diagnosis and therapy have been developed [113]. Nanotechnology also plays an important role in advanced drug-loaded formulations with various functions such as targeting and controlled release [114]. Despite vast research on drug delivery systems, the number of drug-loaded nanoparticles that has reached clinical practice is limited [113, 115, 116]. One main reason for the gap between research and clinical application is the difference between pre-clinical *in vitro* and *in vivo* models and real carcinoma [116, 117].

One common strategy to evaluate anti-cancer activity of drugs and formulations is to use two-dimensional (2D) monolayer cells in culture. The main advantage of 2D cell culture models is the simple and low-cost maintenance of cell culture [118]. Unfortunately, such models cannot accurately select potential anticancer drugs for clinical applications [118, 119]. 2D cell culture models cannot mimic the natural structures of tissues or solid tumors due to the lack of cell-cell and cell-extracellular environment interactions [118]. These interactions play vital roles for cellular functions such as cell differentiation, proliferation, vitality, and expression of genes and proteins [120, 121].

Compared with the 2D cancer cell monolayers, the 3D multicellular spheroids (3D MCS) contain many features of solid tumors [106]. As shown in Figure 14, the 2D cell culture models cause the cells to expand on a flat surface while 3D cell culture models cause the cells to form 3D spheroids that contain ECM [122]. 3D MCS can also mimic the characteristics of solid

tumors in patients and can create substantial barriers for drugs to penetrate[117]. When MCS grow larger than 500 μm in diameter, they typically develop a necrotic core [123] and hollow, concentric structures, including an outer layer of proliferating cells (proliferation zone), a middle layer of quiescent cells, and a necrotic center of dead or dying cells [124]. A schematic diagram of such structure of 3D MCS is shown in Figure 14 (C). The various stages of cells within the 3D MCS are established because of different gradients of oxygen and nutrients [119]. Furthermore, 3D MCS can be cultured *in vitro* for several weeks for long-term research and can be developed into co-culture models together with other cells to better simulate cell-cell interactions [118, 123]. Therefore, compared with the traditional 2D cell culture models, the 3D MCS not only provide material and structural basis of the microenvironment, but also maintains the physiological functions of tumor cells. 3D MCS are a powerful model for evaluating the clinical efficacy of anticancer drug candidates [122]. 3D MCS models have been also widely used in preclinical studies on drug-loaded nano delivery systems [116].

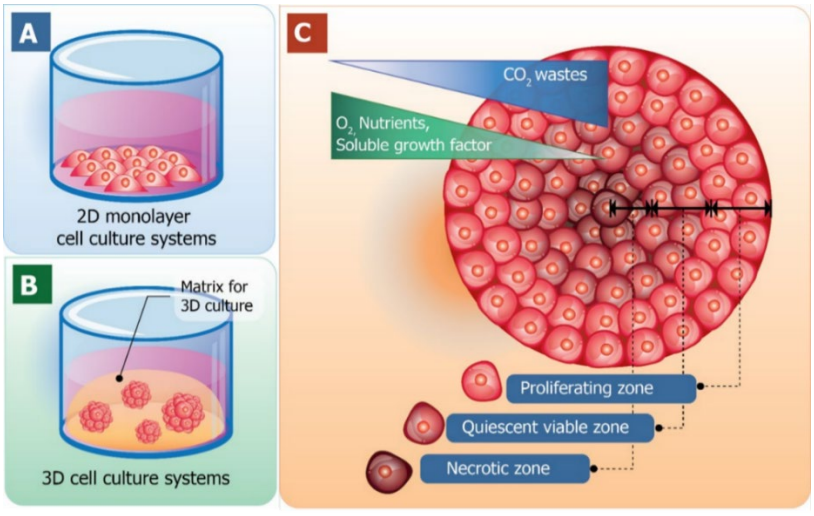


*Figure 14.* Schematic diagrams of traditional 2D monolayer cell cultures (A) and 3D cell cultures (B, C). Adapted from [122].

As reported in this chapter and shown in Figure 15, non-small cell lung cancer cells (A549 and A549-iRFP) were constructed into 3D MCS and then used to evaluate the anticancer activity of Miriplatin-loaded formulations.

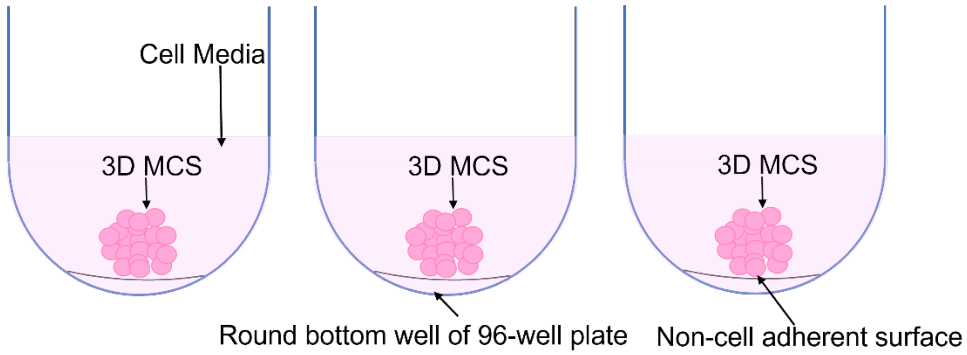


*Figure 15.* A Schematic diagram of 3D MCS established by seeding cells into 96-well microplate plates with non-adherent surfaces.

The objective of this chapter is to evaluate the anticancer activity of Miriplatin-loaded formulations in 3D MCS models.

## 4.2 Materials and Methods

### 4.2.1 Cell Line and Reagents

Human lung adenocarcinoma A549-iRFP cell line (λex =690 nm, λem = 713 nm) was purchased from Imanis Life Sciences (MN, US). Human lung adenocarcinoma A549 cell line was purchased from ATCC (VA, US). Cell culture reagents, if not specified, were purchased from Corning Life Science. A549-iRFP was grown in DMEM cell culture media with 10% Fetal bovine serum (Sigma-Aldrich, US), 1% penicillin-streptomycin (Corning Life Science, US), and 1 µg/ml puromycin (Alfa Aesar, US). A549 cells were grown in RPMI cell culture media supplemented with 10% Fetal bovine serum (Gemini Bio-Products, CA) and 1% penicillin-

streptomycin. Falcon® 96-well Black/Clear Flat Bottom Microplate and 96-well Spheroid Microplate were purchased from Coring Life Science. Tumor spheroids were constructed with 0.3% collagen, which was purchased from Fisher Scientific (PA, US). All cells were maintained at 37 ℃ and 5% $CO_2$ in cell incubator. The viability of MCS was measured by CellTiter-Glo® 3D Reagent (Promega Corporation, US).

### 4.2.2 Establishment of 3D MCS

A549 and A549-iRFP cells were seeded into 96-well spheroid microplates at 3000 cells/well in 100 μL/well of the aforementioned growth media that was supplemented with 0.3% collagen (Gibco, US). The microplates were centrifuged at 4 ℃, 300 g for 7 minutes on an Eppendorf Centrifuge 5810R to facilitate the cell-cell aggregation. The cells were cultured for 48 hours and then supplemented with another 100 μL/well growth media without collagen. Every two days thereafter, 100 μL of the growth medium in each well was replaced with equal volume (100 μL) of fresh growth medium without collagen to maintain a 200 μL total media volume.

### 4.2.3 Morphology of 3D MCS

The morphology and growth of 3D MCS were monitored by a Keyence (US) BZ-X700 fluorescence microscope.

### 4.2.4 Fluorometric Characterization of 3D MCS

The fluorescent signal ($\lambda ex$ = 685 nm, $\lambda em$ = 700 nm) was traced by Odyssey® Infrared Imaging 205 System (LI-COR® Biosciences, Lincoln, NE, USA) at the 700 nm channel.

### 4.2.5 Cell Viability Assays for 3D MCS

For the viability assay, 3D MCS of A549 or A549-iRFP cells (3000 seeded cells/well) were transferred from the original 96-well spheroid microplates to an opaque-walled 96-well

plate with 100 μL fresh media. An equal volume (100 μL) of CellTiter-Glo 3D Cell Viability Assay reagent (Promega Corporation, WI, USA) was added into each well. The plate was shaken for 5 min and incubated at room temperature for an additional 25 min to achieve stable luminescent signals. The luminescence was then detected by a Synergy HTX microplate reader (BioTek, US).

### 4.2.6 Treatment of 3D MCS with Miriplatin-loaded Formulations

A549 and A549-iRFP cells (3000 cells/well) within 15 passages were seeded into 96-well spheroid microplates to develop 3D MCS by the method described above. Among different batches, A549 and A549-iRFP cells used for biological replicates were within 5 passages. After 6-8 days, 3D MCS grew to about 500 μm in diameter. Then 3D MCS were treated with free drugs (such as Cisplatin, Miriplatin, Paclitaxel) and Miriplatin-loaded formulations. The input concentration of platinum or Paclitaxel in free drugs and formulations was controlled to be equal. Cisplatin was directly dissolved into complete media while Miriplatin and Paclitaxel were dissolved into complete media containing 1% DMSO (dimethyl sulfoxide). All media containing free drugs or formulations were vortexed and mixed uniformly before treatment. 3D MCS were treated for 7 days including 3-day exposure to drug or formulations and 4-day growth in platinum-free growth media. Specifically, after incubation in growth media containing drug or drug formulation for 3 days at 37 °C, 5% $CO_2$, the growth media in each well was completely removed and replaced by 200 μL fresh growth media. In case there was any sediment at the bottom of wells, it was carefully suspended and removed together with the growth media using a pipette. After the cells were cultured for another 2 days, 100 μL of growth media was replaced by 100 μL fresh growth media to maintain a total 200 μL media volume per well. The 3D MCS were incubated for another 2 days.

Compared with the traditional three-day drug exposure treatment, the modified treatment method added 4 more days of drug-free growth in order to screen the fluorescent signals of 3D MCS to monitor whether cancer cells will recur after drug exposure. This modification aimed to mimic clinical regimens in which patients rest for several weeks between each round of chemotherapy while continuously monitoring the efficacy and toxicity.

### 4.2.7 Evaluation of the Anti-cancer Activity of Miriplatin-loaded Formulations

The fluorescence signal of A549-iRFP 3D MCS was monitored daily during the 7-day treatment. The fluorescence signal of 3D MCS treated with growth medium alone in the same 96-well plate is used as a reference for 100% viability (0% growth inhibition). The formula for calculating 3D MCS viability% of each treatment group (free drugs and formulations) by fluorescence signal (n=4) is as follows:

$$3D\ MCS\ viability\ (\%)\ by\ fluorescence\ signal = \frac{Fluorescence\ signal\ from\ 3D\ MCS\ (treatment\ group)}{Fluorescence\ signal\ from\ 3D\ MCS\ (medium\ group)} \times 100\%$$

Recording 3D MCS viability% for each group daily, the growth of 3D MCS during the 7-day treatment was traced. A treatment group with lower 3D MCS viability% at Day 7 was considered to have better anti-cancer activity.

The luminescence of 3D MCS (A549-iRFP or A549) was measured at Day 7. The luminescence signal of 3D MCS treated with growth medium alone in the same 96-well plate is used as a reference for 100% 3D MCS viability (0% growth inhibition). The formula for calculating 3D MCS viability% of each treatment group by 3D MCS Viability Assay (n=4) is as follows:

$$3D\ MCS\ viability\ (\%)\ by\ \text{3D MCS Viability Assay} = \frac{\text{Luminescence}\ from\ 3D\ MCS\ \ (treatment\ group)}{\text{Luminescence}\ from\ \ 3D\ MCS\ \ (medium\ group)} \times 100\%$$

Lower 3D MCS viability% at Day 7 would indicates better anti-cancer activity.

3D MCS viability% by fluorescent signal and 3D MCS viability% by 3D MCS Viability Assay were both included as triangulated evaluation anti-cancer activity of Miriplatin-loaded formulations. The former was carried out each day during the period of 7-day treatment and the latter at the end of the 7-day treatment (Day 7).

The 3D MCS growth inhibition by Miriplatin-loaded formulations is calculated by the formula below:

$$3D\ MCS\ Inhibition\ (\%) = 100\% - 3DMCS\ Viability\ (\%)$$

**4.2.8 Dose-dependent MCS Growth Inhibition by Miriplatin-loaded Formulations**

A549-iRFP cells (3000 cells/well) were seeded into 96-well spheroid microplates. After 6-8 days, 3D MCS grew to about 500 μm in diameter. Then the 3D MCS was treated by free Cisplatin and Miriplatin-loaded formulations using the 7-day treatment method as described earlier. The input concentrations of platinum were 1, 5, 10, 20, 40, 60, 80, 100, 200, and 400 μM. The fluorescent signal of A549-iRFP 3D MCS was monitored daily during the 7-day treatment. The luminescence of 3D MCS was analyzed by 3D MCS Viability Assay at Day 7. The 3D MCS growth inhibition by a drug or formulation treatment was calculated by the above formula. Half maximal inhibitory concentration ($IC_{50}$) value measures the effectiveness of a treatment to inhibit MCS growth [125]. The $IC_{50}$ value (μM) of each treatment was calculated from the dose-dependent growth inhibition data by nonlinear regression [log(inhibitor) vs. response, Variable slope, four parameters] using GraphPad Prism 8.0 Software.

## 4.3 Results and Discussion

### 4.3.1 Morphology of 3D MCS

The 3D MCS models of two non-small cell lung cancer cell lines (A549 and A549-iRFP) were successfully established at selected seeding density (3000 cells/well) with centrifugation and collagen addition in the growth media.

As shown in Figure 16, 3D MCS had a morphology of a tight and round structure in 17 days. The edge of 3D MCS was smooth and clear in the first 11 days. Then rough edge of 3D MCS could be observed since Day 13. After 5 to 7 days, 3D MCS grew to about 500 μm in diameter. From Day 5, a lighter grey central core could be observed, which was also discussed by other researchers [123, 124]. When 3D MCS became larger than 500 μm in diameter, a central necrosis typically appeared. The structures of 3D MCS turned into hollow center structures, including an outer layer of proliferating cells (proliferation zone), a middle layer of quiescent cells and a necrotic center of dead or dying cells[124].

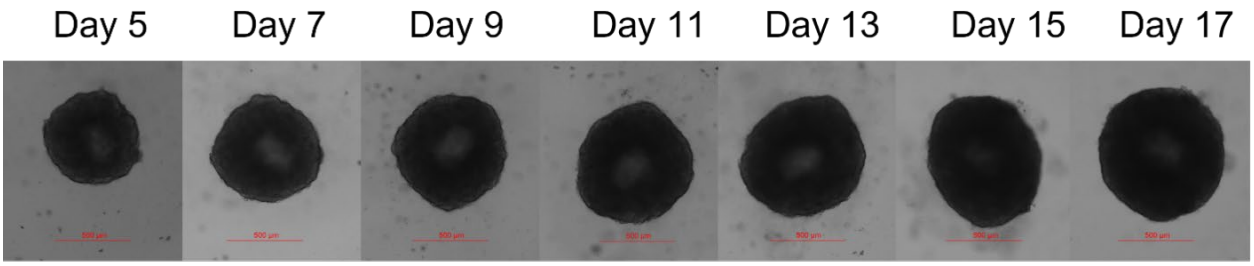


*Figure 16.* Morphology of A549-iRFP 3D MCS (3000 seeded cells/well) after 5, 7, 9, 11, 13, 15, 17 days of culturing (scale bar=500 μm).

### 4.3.2 Comparison between the Viability of A549 and A549-iRFP 3D MCS after Anti-cancer Treatment

To compare 3D MCS viability results between A549 and A549-iRFP cell line by 3D Viability assay, 3D MCS models of A549 and A549-iRFP were established for 7-day anti-cancer treatments. Treatment groups included free Cisplatin, free Paclitaxel (PTX), Miriplatin-loaded SLNs, and PTX-loaded SLNs. As shown in Figure 17, 3D MCS viability results of A549 and A549-iRFP 3D MCS were similar under different treatments. Therefore, the 3D MCS of A549-iRFP could serve as a valid lung cancer model for evaluation of anti-cancer activity of chemotherapeutic agents and drug-loaded formulations.

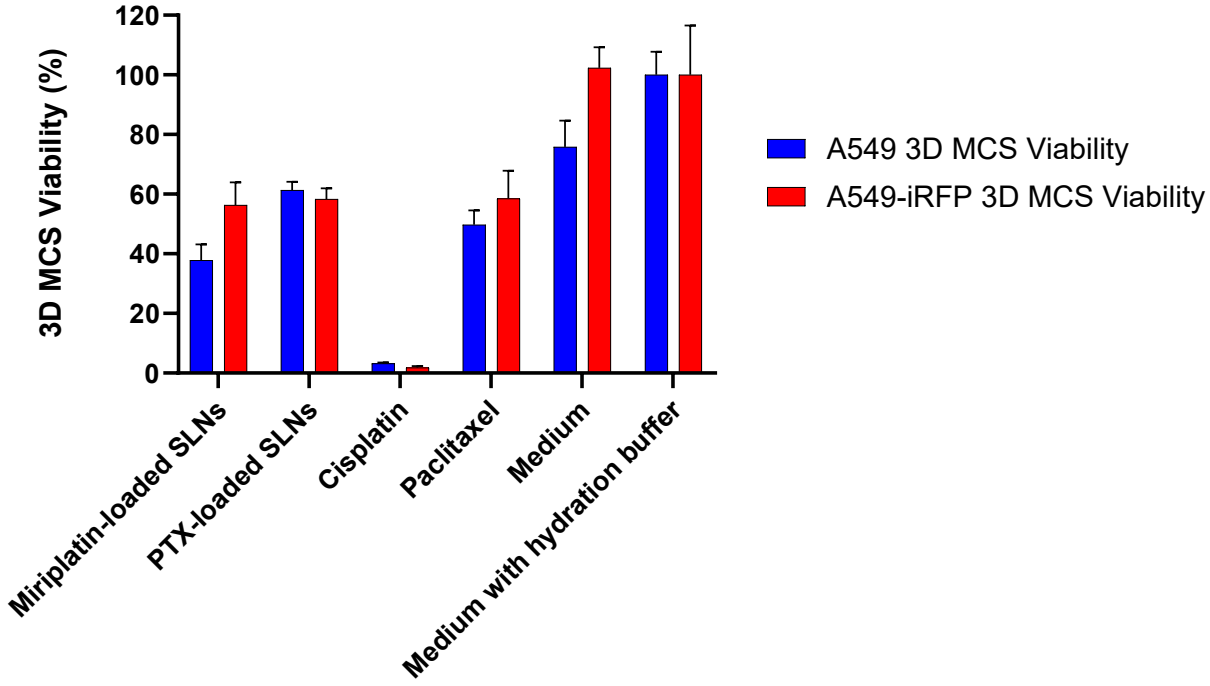


*Figure 17.* 3D MCS viability of A549 (blue) and A549-iRFP (red) after treatment with anticancer drugs and drug formulations (mean ± S. D, n = 4). Drug concentrations of each treatment groups were same (400μM).

### 4.3.3 Comparison of Anti-cancer Activity of Miriplatin-loaded Formulations with Different Molar Ratio of PE-PEG$_{2000}$

To compare the anti-cancer activity of Miriplatin-loaded formulations with different molar ratios of PE-PEG$_{2000}$ at same input platinum concentration (400 μM), 3D MCS viability of A549-iRFP after 7-day treatments was quantified by 3D MCS Viability Assay and fluorometry. As shown in Figure 4.5, as the molar ratio of PE-PEG$_{2000}$ to TP and Miriplatin increased from 1:9:2to 4:6:2, the 3D MCS viability of A549-iRFP by 3D MCS Viability Assay decreased from about 40% to 0%. The 3D MCS viability by fluorescent signals showed similar trend. This indicates that PE-PEG$_{2000}$ could facilitate the preparation of Miriplatin-loaded formulations. Due to the structure of PE-PEG$_{2000}$, it has "smoothing" effect to reduce the heterogeneity and the number of cavities in lipid layer surface [126]. Based on the results from chapter 3, Miriplatin-loaded formulations with more molar ratios of PE-PEG$_{2000}$ had smaller sizes, which could improve the penetration and uptake of formulations into 3D MCS [117].

The 3D MCS viability of free Miriplatin treatment group was about 100%, which indicated that Miriplatin did not have any anti-cancer activity in aqueous solution, most probably due to its poor water solubility (mentioned in Chapter 1). As shown in Figure 18, compared with free Miriplatin, Miriplatin-loaded micelles and SLNs caused much lower 3D MCS viability. Therefore, the lipid-based delivery system improved the anti-cancer activity of Miriplatin. Furthermore, the 3D MCS viability of Miriplatin-loaded micelles (PE-PEG$_{2000}$: Miriplatin=10:2) was similar to the viability of free Cisplatin treatment group (close to 0%), suggesting that the micelles have anti- lung cancer activities that is comparable to the currently best drug against non-small cell lung cancer.

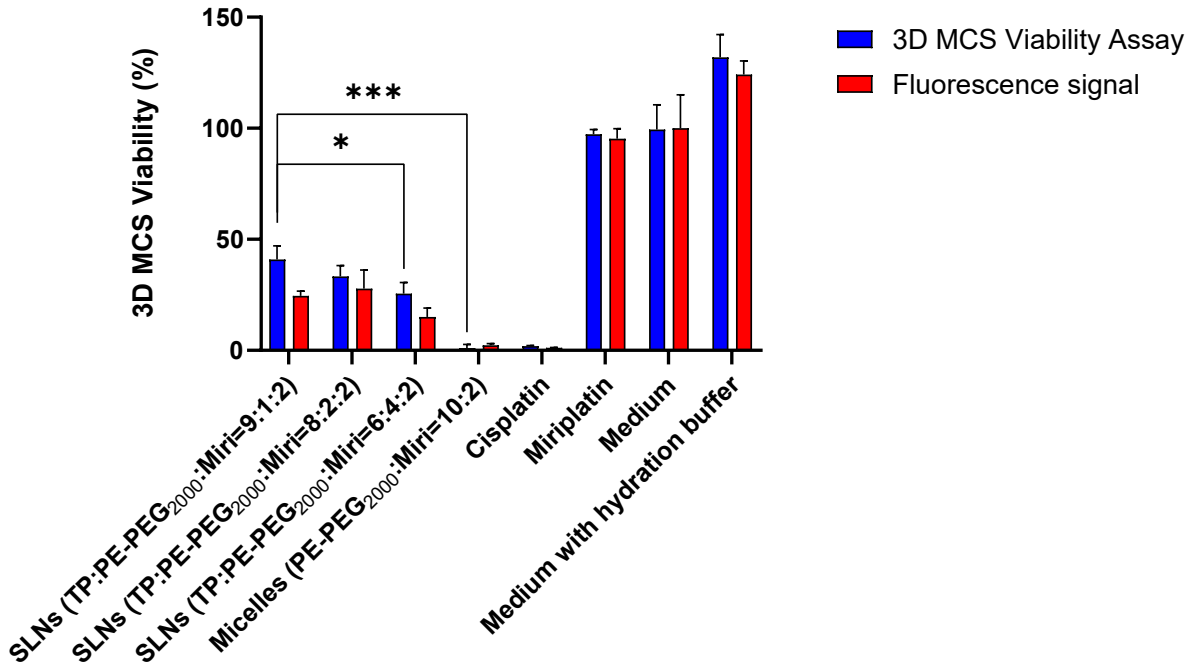


*Figure 18.* 3D MCS Viability of A549-iRFP after treatment of Miriplatin-loaded formulations with different molar ratio of PE-$PEG_{2000}$ (Miri: Miriplatin, mean ± S. D, n = 3). *P<0. 05, ***P<0. 001. Drug concentrations of each treatment groups were same (400μM).

### 4.3.4 Comparison of Anti-cancer Activity of Miriplatin-loaded Formulations with Different Molar Ratio of Miriplatin

To compare the anti-cancer activity of formulations of the same platinum concentration during preparation (400 μM) but at different molar ratio relative to other lipid components, 3D MCS viability of A549-iRFP after 7-day treatments by the 3D MCS Viability Assay and the fluorescent signals is shown in Figure 19. For Miriplatin-loaded micelles, as the molar ratio of Miriplatin to PE-$PEG_{2000}$ increased from 1:10 to 2:10, the 3D MCS viability of A549-iRFP by 3D MCS Viability Assay significantly decreased from about 25% to 0%. The 3D MCS viability by fluorescent signals had similar results. The comparison between SLNs showed similar trend.

Therefore, increasing molar ratio of Miriplatin in compositions improved the anti-cancer activity of Miriplatin-loaded formulations.

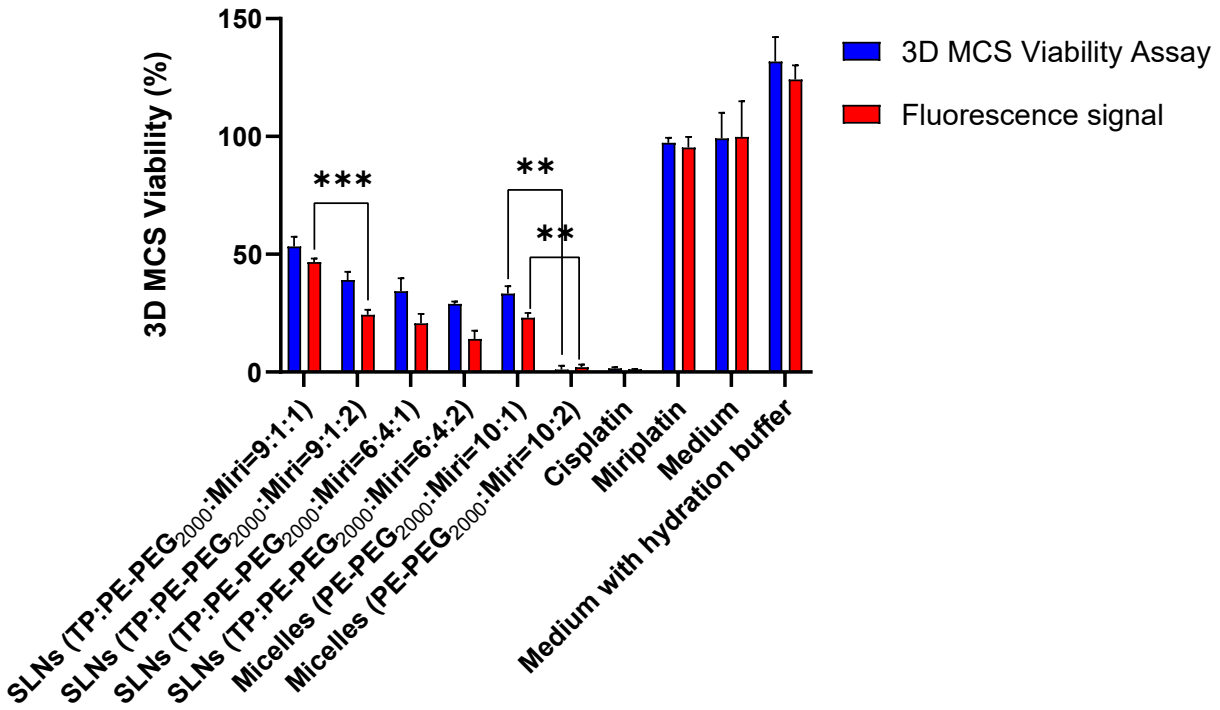


*Figure 19.* Comparison of 3D MCS viability of A549-iRFP after treatment with Miriplatin-loaded formulations at different molar ratios of Miriplatin (Miri: Miriplatin, mean ± S. D, n = 3). **P<0. 01, ***P<0. 001. Drug concentrations of each treatment groups were same (400μM).

### 4.3.5 Comparison of Anti-cancer Activity of Miriplatin-loaded Micelles and SLNs

The viability of A549-iRFP 3D MCS treated with Miriplatin-loaded micelles and SLNs is shown in Figure 20. The recovery rates of intact Miriplatin from Miriplatin-loaded formulations were quantified by HPLC. In order to better corelate anticancer activity and recovery rates of intact Miriplatin from formulations, 3D MCS viability was converted to 3D MCS growth inhibition by the formula mentioned above (Section 4.2.7). As shown in Figure 21, there was a

strong relationship between the recovery of intact Miriplatin from Miriplatin-loaded formulations and their anticancer activity as determined by both 3D MCS Viability Assay and by iRFP fluorescence signal. Miriplatin-loaded micelles with higher recovery of intact Miriplatin had higher anticancer activity than Miriplatin-loaded SLNs with lower recovery. Together, the recovery of intact Miriplatin and the biological activity results suggest that Miriplatin-loaded micelles have better anti-cancer activity against A549-iRFP 3D MCS.

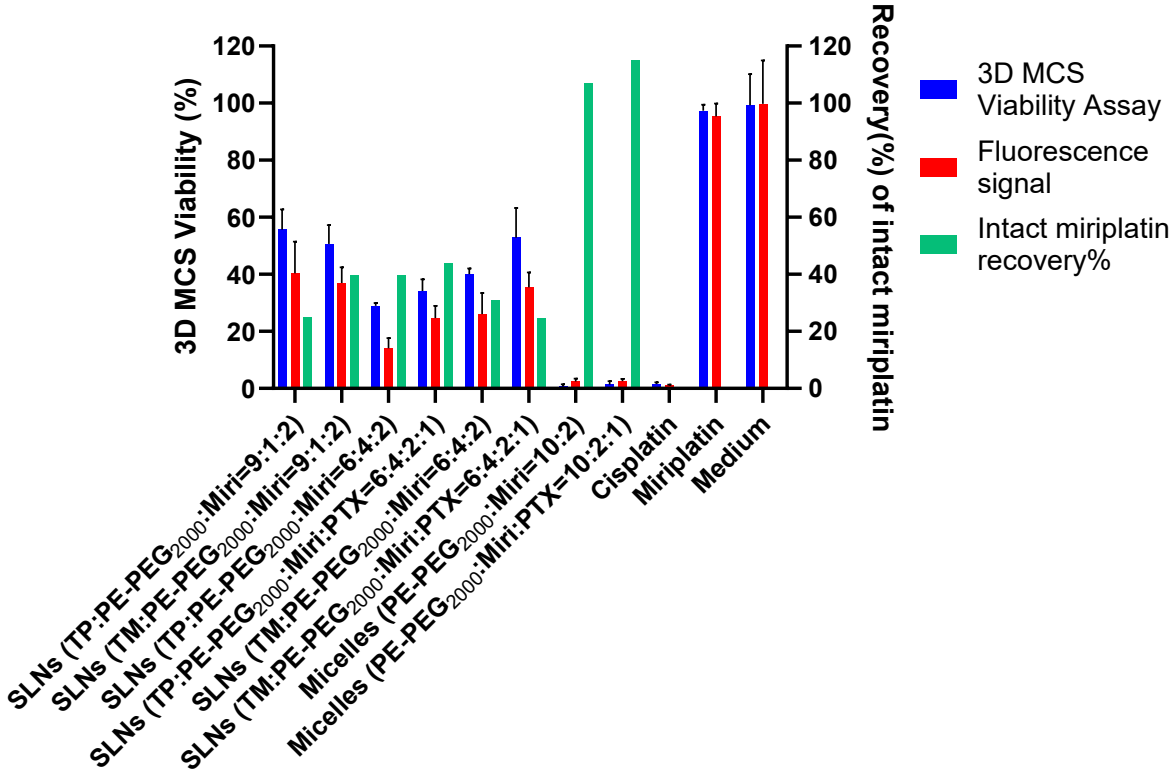


*Figure 20.* Viability of A549-iRFP 3D MCS after treatment with Miriplatin-loaded formulations per 3D MCS Viability Assay (blue) and iRFP fluorescence (red) (Mean ± S. D, n = 4) In Comparison to the recovery of intact Miriplatin from each formulation (green) (Miri: Miriplatin, PTX: Paclitaxel). Drug concentrations of each treatment groups were same (400µM).

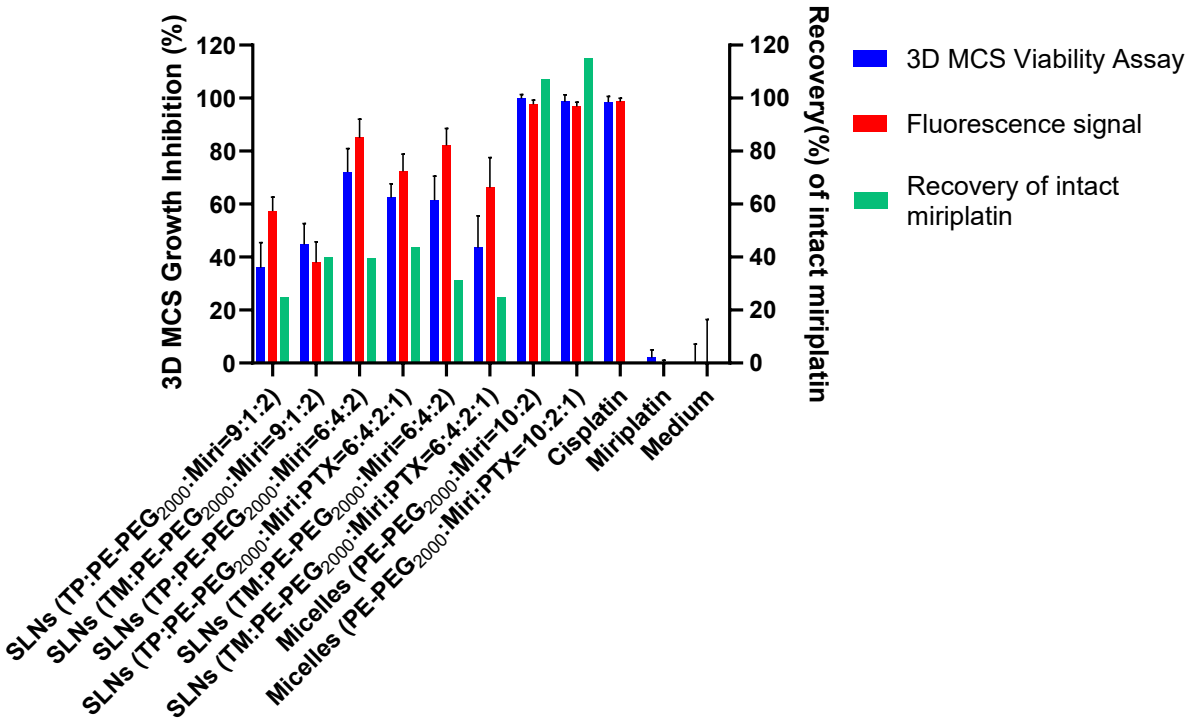


*Figure 21.* Growth inhibition of A549-iRFP MCS after treatment with Miriplatin-loaded formulations per 3D MCS Viability Assay (blue) and iRFP fluorescence (red) (mean ± S. D, n = 4). In comparison to recovery of intact Miriplatin from each formulation (green) (Miri: Miriplatin, PTX: Paclitaxel). Drug concentrations of each treatment groups were same (400µM).

### 4.3.6 Dose-dependent Growth Inhibition of A549-iRFP MCS by Miriplatin-loaded Micelles

Viability of A549-iRFP 3D MCS after 7-day treatment was quantified by 3D MCS Viability Assay. As shown in Figure 22, 3D MCS viability decreased as the platinum concentration of treatment increased. The 3D MCS growth inhibition values were calculated from viability by the formula mentioned above (Section 4.2.7). As shown in Figure 23, in the concentration range of 10 µM to 100 µM, the growth inhibition of treatment groups increased faster than in other concentration ranges.

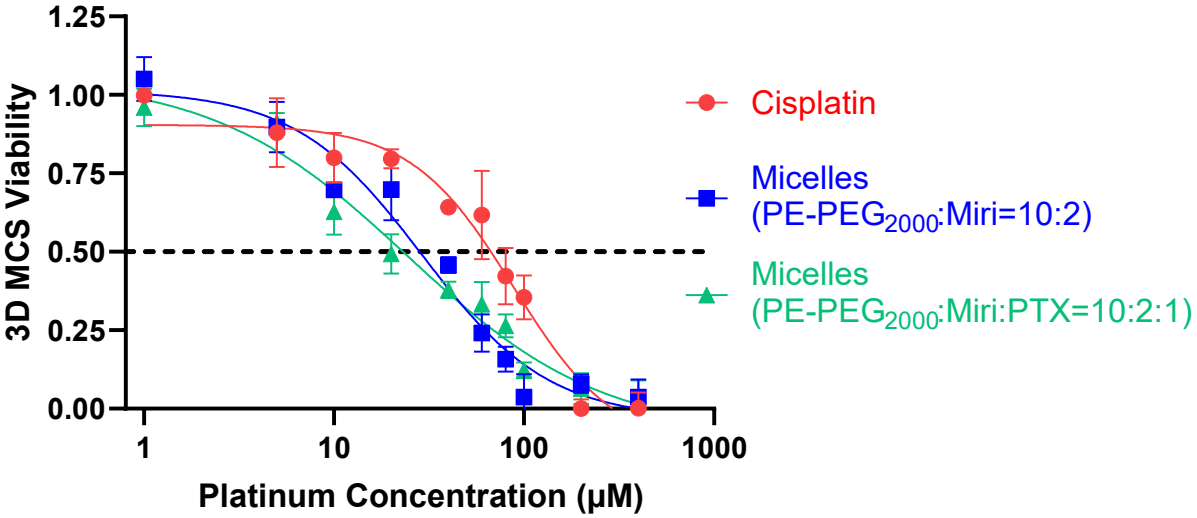


*Figure 22.* Viability of A549-iRFP 3D MCS treated with Miriplatin-loaded micelles and Cisplatin solution per 3D MCS Viability Assay (mean ± S. D, n = 3). (Miri: Miriplatin, PTX: Paclitaxel)

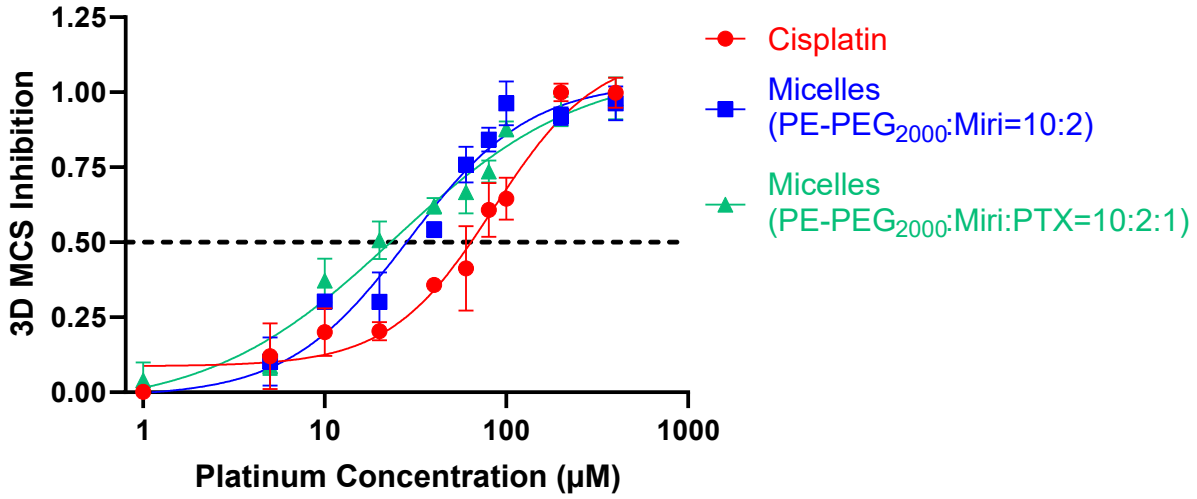


*Figure 23.* Growth inhibition of A549-iRFP 3D MCS by Miriplatin-loaded micelles and Cisplatin solution per 3D MCS Viability Assay (mean ± S. D, n = 3). (Miri: Miriplatin, PTX: Paclitaxel)

The $IC_{50}$ value of two types of Miriplatin-loaded micelles (either Miriplatin alone or Miriplatin together with Paclitaxel) and Cisplatin solution by 3D MCS Viability Assay are listed in Table 19. The $IC_{50}$ value of micelles loaded with both Miriplatin, and Paclitaxel was 24.37 μM, which is smaller than that of micelles loaded with only Miriplatin (29.02 μM). The $IC_{50}$ value of free Cisplatin (84.78 μM) was much larger than those of the two types of Miriplatin-loaded micelles. This indicates that Miriplatin-loaded micelles have better anti-cancer activity on A549-iRFP 3D MCS than Cisplatin, which is a benchmark due to its wide use against NSCLC in clinic.

Table 19

*$IC_{50}$ Value of Miriplatin-loaded Micelles and Cisplatin Solution*

| **Treatment Groups** | **IC50 Value Determined by Data from 3D MCS Viability Assay (μM)** | **P Value by T-test** |
|---|---|---|
| Cisplatin | 84.78 | - |
| Micelles (PE-$PEG_{2000}$: Miri=10:2) | 29.02 | <0.0001 |
| Micelles (PE-$PEG_{2000}$: Miri: PTX=10:2:1) | 24.37 | 0.0249 |

(Miri: Miriplatin, PTX: Paclitaxel)

## 4.4 Summary

3D MCS of A549-iRFP and A549 were successfully established as models of NSCLC to evaluate anti-cancer activities of Miriplatin-containing micelles in vitro. The viability of A549-iRFP 3D MCS was similar to that of A549 3D MCS after 7-day treatment by Miriplatin-loaded formulations or free drugs. The A549-iRFP 3D MCS viability by 3D MCS Viability Assay and iRFP fluorescence signal had similar trends in different treatment groups. The anti-cancer

activity of Miriplatin-loaded formulations was positively associated with the recovery of intact Miriplatin from the formulations.

For Miriplatin-loaded SLNs, the anti-cancer activity against A549-iRFP 3D MCS increased when the molar ratio of Miriplatin increased. Miriplatin-loaded SLNs consisting of higher molar ratios of PE-$PEG_{2000}$ also had higher anti-cancer activity.

Miriplatin-loaded micelles inhibited the growth of A549-iRFP 3D MCS much more effectively than Miriplatin-loaded SLNs. Moreover, Miriplatin-loaded micelles had higher anti-cancer activity against A549-iRFP 3D MCS than Cisplatin as a clinical benchmark.

# CHAPTER 5: SUMMARY AND FUTURE WORK

Lung cancer claims the highest mortality and the second-most estimated new cases among all oncological diseases [1]. NSCLC accounts for approximately 85% of all newly diagnosed lung cancers [2]. If the tumor is found to be resectable and the patient can tolerate surgery, patients with stage I, II, and IIIA NSCLC usually undergo surgery to remove the tumor [5]. Approximately 40% of newly diagnosed lung cancer patients are stage IV. For stage IV NSCLC, cytotoxic combination chemotherapy is the first-line therapy [5]. The American Society of Clinical Oncology states that treatment is a regimen of platinum (Cisplatin or Carboplatin) plus Paclitaxel, gemcitabine, docetaxel, vinorelbine, irinotecan, or pemetrexed [3]. Cisplatin is much more effective than other platinum drugs at the same dosage [4], however, Cisplatin has been associated with more side effects and induction of drug resistance [5].

Deep penetration of anticancer drugs into solid tumors is a factor that limits the effectiveness of chemotherapy [8]. Nanoparticles with appropriate properties provide a promising platform to overcome the biological barriers that hinder anti-cancer activity [9]. Miriplatin is a lipophilic anti-cancer drug that has been approved in Japan for transcatheter arterial chemoembolization treatment of hepatocellular carcinoma [6]. Lipid-based nanoparticles such as liposomes, micelles, and solid lipid nanoparticles (SLNs) can encapsulate anti-cancer drugs to improve their water solubility and bioavailability. In this study, Miriplatin was formulated into various micelles, liposomes, and SLNs by film-hydration and evaluated their physicochemical properties and anti-cancer activity against NSCLC cells in culture.

Miriplatin-loaded formulations were successfully prepared by the film-hydration method. The size of the Miriplatin-loaded formulations was characterized by dynamic light scattering

(DLS) and reported using number-weighted distribution. Different compositions of the formulations have been developed. Miriplatin-loaded micelles were much smaller and more homogeneous than Miriplatin-loaded liposomes and SLNs. Most Miriplatin-loaded micelles were about 15 nm in diameter, while SLNs were around 120 nm, and liposomes were about 180 nm. Formulations with a higher molar ratio of PE-$PEG_{2000}$ in the compositions had smaller sizes. SLNs loaded with a higher molar ratio of Miriplatin in the composition showed smaller sizes.

ICP-MS and ICP-OES techniques were attempted to quantify the platinum element in the formulations. Different Miriplatin-loaded formulations were digested by 70% nitric acid and heated at 90 ℃ for 90 min. Formulations with a higher molar ratio of PE-$PEG_{2000}$ in the compositions had more platinum recovery. Most Miriplatin-loaded formulations had higher than 80% platinum recovery.

The recovery of intact Miriplatin was characterized by HPLC. The stationary phase was kept at 25 ℃, and the mobile phase (methanol: water = 92:8, v/v) was run at the flow rate of 1 mL/min. The effluent was monitored at wavelength 210 nm. The retention time of intact Miriplatin was about 9.7 min. For each HPLC sample, 50 μL Miriplatin-loaded formulation was diluted with 950 μL methanol and centrifuged. The supernatant was taken for HPLC analysis. An aliquot (20 μL) of each sample was injected into HPLC after preparation. Miriplatin-loaded micelles had much higher intact Miriplatin recovery (~100%) than SLNs (~30%).

Miriplatin-loaded formulations were negatively stained with uranyl acetate and then imaged by TEM. The micelles showed the morphology of spherical dots of about 10 nm in diameter while SLNs showed both spherical and rodlike structures of about 120 nm in diameter. The TEM results were consistent with the size and PDI results by the Zetasizer.

3D MCS of A549 and A549-iRFP cell lines were successfully established as an in vitro model to evaluate activity against non-small cell lung cancer. The viability of A549-iRFP 3D MCS after 7-day treatment with anticancer drugs or drug formulations was measured by 3D MCS Viability Assay and the fluorescence of iRFP. The growth of A549-iRFP 3D MCS during the anticancer treatment was monitored daily by its iRFP fluorescence. The viability of 3D MCS after 7-day treatment with Miriplatin-loaded micelles was about 0%, which was similar to Cisplatin. Miriplatin-loaded formulations with a higher molar ratio of PE-$PEG_{2000}$ in the compositions had higher anti-cancer activity against 3D MCS. The anticancer activity of Miriplatin-loaded formulations against 3D MCS was positively associated with the recovery of intact Miriplatin from the formulations. The $IC_{50}$ value of Miriplatin-loaded micelles against A549-iRFP 3D MCS was about 25 μM, while that of Cisplatin was about 90 μM.

Future work for further development of Miriplatin-loaded formulations would include optimization of compositions. For example, lecithin can be included into the formulations to increase the drug-loading capacity. Cholesterol myristate can be added into compositions to improve the stability and homogeneity of lipid-based formulations. In addition, Miriplatin-loaded formulations can be modified with targeting ligands to increase accumulation at the lung cancer site.

For application in industry, long-term storage methods such as lyophilization should be considered to reduce the precipitation, enhance the stability, and prolong the storage time of formulations. Moreover, a scale-up preparation method should be developed. Also, the preparation method needs to be improved to reduce batch-to-batch variance.

For the quantification of the encapsulation efficiency of Miriplatin-loaded formulations, it needs to be established a method to separate free drug molecules (such as free Miriplatin) from

drug formulations. After separation, it could quantify the encapsulation efficiency of Miriplatin-loaded formulations and study *in vitro* drug release from Miriplatin-loaded formulations. Also, the calibration curves of different degradation products of Miriplatin such as those losing one or two 14-carbon chains could be established by HPLC so that quantifying different forms of platinum compounds in Miriplatin-loaded formulations can be achieved.

For *in vitro* cell culture studies, Cisplatin-resistant lung cancer cell lines could be used to study possible advantages of Miriplatin-loaded formulations against drug resistance. The penetration of Miriplatin-loaded formulations into 3D MCS could be studied by confocal microscopy. For *in vivo* studies, the distribution, pharmacokinetics, and anticancer efficacy of the formulations could be characterized in animal models of NSCLC.

In summary, the reported lipid-based nanoparticles of Miriplatin represent a promising drug delivery system against NSCLC. Miriplatin-loaded formulations were developed by the film-hydration method. Miriplatin-loaded micelles carry small size, low PDI, high platinum recovery, and almost 100% recovery of intact Miriplatin. Furthermore, the Miriplatin-loaded micelles inhibited the growth of A549 iRFP 3D MCS more potently than the clinical benchmark Cisplatin.

# REFERENCES


1. R.L. Siegel, K.D. Miller, H.E. Fuchs, A. Jemal, Cancer Statistics, 2021, CA Cancer J Clin 71(1) (2021) 7-33.
2. Y.P. Molina JR, Cassivi SD, Schild SE, Adjei AA, Non-small cell lung cancer: epidemiology, risk factors, treatment, and survivorship Mayo Clinic proceedings 83(5):584-594 (2008).
3. G.A. Masters, S. Temin, C.G. Azzoli, G. Giaccone, S. Baker, Jr., J.R. Brahmer, P.M. Ellis, A. Gajra, N. Rackear, J.H. Schiller, T.J. Smith, J.R. Strawn, D. Trent, D.H. Johnson, P. American Society of Clinical Oncology Clinical, Systemic Therapy for Stage IV Non-Small-Cell Lung Cancer: American Society of Clinical Oncology Clinical Practice Guideline Update, J Clin Oncol 33(30) (2015) 3488-515.
4. S.T. Dasari, P. B., Cisplatin in cancer therapy: molecular mechanisms of action, European Journal of Pharmacology 740 (2014) 364-78.
5. C. Zappa, S.A. Mousa, Non-small cell lung cancer: current treatment and future advances, Transl Lung Cancer Res 5(3) (2016) 288-300.
6. M. Hanada, A. Baba, Y. Tsutsumishita, T. Noguchi, T. Yamaoka, N. Chiba, F. Nishikaku, Intra-hepatic arterial administration with Miriplatin suspended in an oily lymphographic agent inhibits the growth of tumors implanted in rat livers by inducing platinum-DNA adducts to form and massive apoptosis, Cancer Chemother Pharmacol 64(3) (2009) 473-83.
7. Y. Li, D. Qian, H.P. Lin, J. Xie, P. Yang, D. Maddy, Y. Xiao, X. Huang, Z. Wang, C. Yang, Nanoparticle-delivered Miriplatin ultrasmall dots suppress triple negative breast cancer lung metastasis by targeting circulating tumor cells, J Control Release 329 (2021) 833-846.
8. D.S.M.C. Jonathan K. Tunggal, Hafsa Shaikh, and Ian F. Tannock, Penetration of Anticancer Drugs through Solid Tissue: A Factor That Limits the Effectiveness of Chemotherapy for Solid Tumors, Clinical Cancer Research 5 (1999) 1583–1586.
9. M. Millard, I. Yakavets, V. Zorin, A. Kulmukhamedova, S. Marchal, L. Bezdetnaya, Drug delivery to solid tumors: the predictive value of the multicellular tumor spheroid model for nanomedicine screening, Int J Nanomedicine 12 (2017) 7993-8007.
10. A.J. Alberg, M.V. Brock, J.G. Ford, J.M. Samet, S.D. Spivack, Epidemiology of lung cancer: Diagnosis and management of lung cancer, 3rd ed: American College of Chest Physicians evidence-based clinical practice guidelines, Chest 143(5 Suppl) (2013) e1S-e29S.
11. T.Y. Chen, Y.H. Fang, H.L. Chen, C.H. Chang, H. Huang, Y.S. Chen, K.M. Liao, H.Y. Wu, G.C. Chang, Y.H. Tsai, C.L. Wang, Y.M. Chen, M.S. Huang, W.C. Su, P.C. Yang, C.J. Chen, C.F. Hsiao, C.A. Hsiung, Impact of cooking oil fume exposure and fume extractor use on lung cancer risk in non-smoking Han Chinese women, Sci Rep 10(1) (2020) 6774.
12. W.D. Travis, E. Brambilla, A.G. Nicholson, Y. Yatabe, J.H.M. Austin, M.B. Beasley, L.R. Chirieac, S. Dacic, E. Duhig, D.B. Flieder, K. Geisinger, F.R. Hirsch, Y. Ishikawa, K.M. Kerr, M. Noguchi, G. Pelosi, C.A. Powell, M.S. Tsao, I. Wistuba, W.H.O. Panel, The 2015 World Health Organization Classification of Lung Tumors: Impact of Genetic, Clinical and Radiologic Advances Since the 2004 Classification, J Thorac Oncol 10(9) (2015) 1243-1260.
13. H. Lemjabbar-Alaoui, O.U. Hassan, Y.W. Yang, P. Buchanan, Lung cancer: Biology and treatment options, Biochim Biophys Acta 1856(2) (2015) 189-210.
14. G.D. Dubin S, Lung Cancer in Non-Smokers, Missouri Medicine 17(4):375-379 (2020).

15. E. Racanelli, A. Jfri, A. Gefri, E. O'Brien, I.V. Litvinov, A. Zubarev, E. Savin, E. Netchiporouk, Cutaneous Squamous Cell Carcinoma in Patients with Hidradenitis Suppurativa, Cancers (Basel) 13(5) (2021).
16. The development of analytical procedures using ICP-OES and ICP-MS for the analysis of trace metals in pharmaceutical formulations, British Journal of Pharmacy 2(2) (2017).
17. K. Rajdev, A.H. Siddiqui, U. Ibrahim, P. Patibandla, T. Khan, D. El-Sayegh, An Unusually Aggressive Large Cell Carcinoma of the Lung: Undiagnosed until Autopsy, Cureus 10(2) (2018) e2202.
18. M.B. Schabath, M.L. Cote, Cancer Progress and Priorities: Lung Cancer, Cancer Epidemiol Biomarkers Prev 28(10) (2019) 1563-1579.
19. J.H. Cho, M. Hamaji, M.S. Allen, S.D. Cassivi, F.C. Nichols, 3rd, D.A. Wigle, K.R. Shen, C. Deschamps, The prognosis of pulmonary metastasectomy depends on the location of the primary colorectal cancer, Ann Thorac Surg 98(4) (2014) 1231-7.
20. Chemotherapy in non-small cell lung cancer: a meta-analysis using updated data on individual patients from 52 randomised clinical trials, Bmj 311(7010) (1995) 899-909.
21. N.Y. Arya Amini, Laurie E Gaspar, Brian Kavanagh and Sana D Karam, Stereotactic Body Radiation Therapy (SBRT) for lung cancer patients previously treated with conventional radiotherapy: a review. , Radiat Oncology 9:210 (2014).
22. R.D. Schreiber, L.J. Old, M.J. Smyth, Cancer immunoediting: integrating immunity's roles in cancer suppression and promotion, Science 331(6024) (2011) 1565-70.
23. G.V. Scagliotti, F. De Marinis, M. Rinaldi, L. Crino, C. Gridelli, S. Ricci, E. Matano, C. Boni, M. Marangolo, G. Failla, G. Altavilla, V. Adamo, A. Ceribelli, M. Clerici, F. Di Costanzo, L. Frontini, M. Tonato, P. Italian Lung Cancer, Phase III randomized trial comparing three platinum-based doublets in advanced non-small-cell lung cancer, J Clin Oncol 20(21) (2002) 4285-91.
24. F. Fossella, J.R. Pereira, J. von Pawel, A. Pluzanska, V. Gorbounova, E. Kaukel, K.V. Mattson, R. Ramlau, A. Szczesna, P. Fidias, M. Millward, C.P. Belani, Randomized, multinational, phase III study of docetaxel plus platinum combinations versus vinorelbine plus Cisplatin for advanced non-small-cell lung cancer: the TAX 326 study group, J Clin Oncol 21(16) (2003) 3016-24.
25. C. Gridelli, A. Ardizzoni, T. Le Chevalier, C. Manegold, F. Perrone, N. Thatcher, N. van Zandwijk, M. Di Maio, O. Martelli, F. De Marinis, Treatment of advanced non-small-cell lung cancer patients with ECOG performance status 2: results of an European Experts Panel, Ann Oncol 15(3) (2004) 419-26.
26. R.J. Browning, P.J.T. Reardon, M. Parhizkar, R.B. Pedley, M. Edirisinghe, J.C. Knowles, E. Stride, Drug Delivery Strategies for Platinum-Based Chemotherapy, ACS Nano 11(9) (2017) 8560-8578.
27. M. Peyrone, Ueber die Einwirkung des Ammoniaks auf Platinchlorür, Justus Liebigs Annalen der Chemie 51(1): 1-29. (1844).
28. C. Monneret, Platinum anticancer drugs. From serendipity to rational design, Ann Pharm Fr 69(6) (2011) 286-95.
29. Z.H. Siddik, Cisplatin: mode of cytotoxic action and molecular basis of resistance, Oncogene 22(47) (2003) 7265-79.
30. D.W. Shen, L.M. Pouliot, M.D. Hall, M.M. Gottesman, Cisplatin resistance: a cellular self-defense mechanism resulting from multiple epigenetic and genetic changes, Pharmacol Rev 64(3) (2012) 706-21.

31. S.A. Aldossary, Review on Pharmacology of Cisplatin: Clinical Use, Toxicity and Mechanism of Resistance of Cisplatin, Biomedical and Pharmacology Journal 12(1) (2019) 07-15.
32. J.T.H.H.-P. Lipp, Toxicity of platinum compounds, Expert Opinion on Pharmacotherapy 4:6 (2003) 889-901.
33. A.M. Florea, D. Busselberg, Cisplatin as an anti-tumor drug: cellular mechanisms of activity, drug resistance and induced side effects, Cancers (Basel) 3(1) (2011) 1351-71.
34. T. Makovec, Cisplatin and beyond: molecular mechanisms of action and drug resistance development in cancer chemotherapy, Radiol Oncol 53(2) (2019) 148-158.
35. A.P. Silverman, W. Bu, S.M. Cohen, S.J. Lippard, 2.4-A crystal structure of the asymmetric platinum complex [Pt(ammine)(cyclohexylamine)]2+ bound to a dodecamer DNA duplex, J Biol Chem 277(51) (2002) 49743-9.
36. B. Rosenberg, Cisplatin: Its history and possible mechanisms of action." . ,, Cisplatin, Academic
37. L. Drougge, and Lars I. Elding. , "Mechanisms for oxidative addition of molecular chlorine to tetracyanoplatinate (II). Formation of trans-dichlorotetracyanoplatinate (IV) via a platinum (III) intermediate, Inorganic Chemistry 27(5) (1988) 795-798.
38. J.J. Wilson, S.J. Lippard, Synthetic methods for the preparation of platinum anticancer complexes, Chem Rev 114(8) (2014) 4470-95.
39. N.J. Wheate, S. Walker, G.E. Craig, R. Oun, The status of platinum anticancer drugs in the clinic and in clinical trials, Dalton Trans 39(35) (2010) 8113-27.
40. C. Feng, Approaches to the Search of Platinum Anticancer Agents: Derivatizing Current Drugs and Incorporating HDAC Inhibition, Pharmaceutical and Chemical Sciences, University of the Pacific, 2019.
41. M.D.A. William P. McGuire, Carboplatin Substitution for Cisplatin in the Treatment of Ovarian Carcinoma— A Word of Caution, Journal of the National Cancer Institute 81(19) (1989) 1438–1439.
42. O.W. Rixe O, Alvarez M, Parker R, Reed E, Paull K, Fojo T. , Oxaliplatin, tetraplatin, Cisplatin, and Carboplatin: spectrum of activity in drug-resistant cell lines and in the cell lines of the National Cancer Institute's Anticancer Drug Screen panel, Biochem Pharmacol 52(12) (1996) 1855-65.
43. D.C.a.L.R.W. Christine R. Culy, Oxaliplatin, Drugs,60(4) (2000) 895-924.
44. B. Stordal, N. Pavlakis, R. Davey, Oxaliplatin for the treatment of Cisplatin-resistant cancer: a systematic review, Cancer Treat Rev 33(4) (2007) 347-57.
45. T.K. Kazunari Tanaka, Jin Shimakura,Mitsuharu Hanada, Development of Miriplatin, a Novel Antitumor Platinum for Hepatocellular Carcinoma, R&D Report "SUMITOMO KAGAKU" (English Edition) 2011-I, Report 4.
46. O. Tredan, C.M. Galmarini, K. Patel, I.F. Tannock, Drug resistance and the solid tumor microenvironment, J Natl Cancer Inst 99(19) (2007) 1441-54.
47. J. Pineiro Fernandez, K.A. Luddy, C. Harmon, C. O'Farrelly, Hepatic Tumor Microenvironments and Effects on NK Cell Phenotype and Function, Int J Mol Sci 20(17) (2019).
48. S.A.H. Beverly A. Teicher, Antoine Al-Achi and Terence S. Herman, Classification of Antineoplastic Treatments by Their Differential Toxicity toward Putative Oxygenated and Hypoxic Tumor Subpopulations in Vivo in the FSaIIC Murine Fibrosarcoma, Cancer research 50(11) (1990) 3339-3344.

49. K. Graham, E. Unger, Overcoming tumor hypoxia as a barrier to radiotherapy, chemotherapy and immunotherapy in cancer treatment, Int J Nanomedicine 13 (2018) 6049-6058.
50. V. CL., Progress in Nanomedicine: Approved and Investigational Nanodrugs, P & T : a peer-reviewed journal for formulary management 42(12) (2017) 742-755.
51. T.T.H. Thi, E.J.A. Suys, J.S. Lee, D.H. Nguyen, K.D. Park, N.P. Truong, Lipid-Based Nanoparticles in the Clinic and Clinical Trials: From Cancer Nanomedicine to COVID-19 Vaccines, Vaccines (Basel) 9(4) (2021).
52. C.P. Balamurugan K, Lipid nano particulate drug delivery: An overview of the emerging trend, .Pharma Innovation 2018 7(7) (2018) 779-789.
53. E. Beltrán-Gracia, A. López-Camacho, I. Higuera-Ciapara, J.B. Velázquez-Fernández, A.A. Vallejo-Cardona, Nanomedicine review: clinical developments in liposomal applications, Cancer Nanotechnology 10(1) (2019).
54. J.O. Eloy, M. Claro de Souza, R. Petrilli, J.P. Barcellos, R.J. Lee, J.M. Marchetti, Liposomes as carriers of hydrophilic small molecule drugs: strategies to enhance encapsulation and delivery, Colloids Surf B Biointerfaces 123 (2014) 345-63.
55. S. Shah, V. Dhawan, R. Holm, M.S. Nagarsenker, Y. Perrie, Liposomes: Advancements and innovation in the manufacturing process, Adv Drug Deliv Rev 154-155 (2020) 102-122.
56. J. Bourquin, A. Milosevic, D. Hauser, R. Lehner, F. Blank, A. Petri-Fink, B. Rothen-Rutishauser, Biodistribution, Clearance, and Long-Term Fate of Clinically Relevant Nanomaterials, Adv Mater 30(19) (2018) e1704307.
57. J.C. Kraft, J.P. Freeling, Z. Wang, R.J. Ho, Emerging research and clinical development trends of liposome and lipid nanoparticle drug delivery systems, J Pharm Sci 103(1) (2014) 29-52.
58. Y. Zhang, Y. Huang, S. Li, Polymeric micelles: nanocarriers for cancer-targeted drug delivery, AAPS PharmSciTech 15(4) (2014) 862-71.
59. Y. Lu, E. Zhang, J. Yang, Z. Cao, Strategies to improve micelle stability for drug delivery, Nano Res 11(10) (2018) 4985-4998.
60. T. Wei, C. Chen, J. Liu, C. Liu, P. Posocco, X. Liu, Q. Cheng, S. Huo, Z. Liang, M. Fermeglia, S. Pricl, X.J. Liang, P. Rocchi, L. Peng, Anticancer drug nanomicelles formed by self-assembling amphiphilic dendrimer to combat cancer drug resistance, Proc Natl Acad Sci U S A 112(10) (2015) 2978-83.
61. H. Cabral, M. Murakami, H. Hojo, Y. Terada, M.R. Kano, U.I. Chung, N. Nishiyama, K. Kataoka, Targeted therapy of spontaneous murine pancreatic tumors by polymeric micelles prolongs survival and prevents peritoneal metastasis, Proc Natl Acad Sci U S A 110(28) (2013) 11397-402.
62. J. Wang, Weiwei Mao, Lye Lin Lock, Jianbin Tang, Meihua Sui, Weilin Sun, Honggang Cui, Dong Xu, and Youqing Shen. , The role of micelle size in tumor accumulation, penetration, and treatment ACS nano 9(7) (2015) 7195-7206.
63. M. Geszke-Moritz, M. Moritz, Solid lipid nanoparticles as attractive drug vehicles: Composition, properties and therapeutic strategies, Mater Sci Eng C Mater Biol Appl 68 (2016) 982-994.
64. V.A. Duong, T.T. Nguyen, H.J. Maeng, Preparation of Solid Lipid Nanoparticles and Nanostructured Lipid Carriers for Drug Delivery and the Effects of Preparation Parameters of Solvent Injection Method, Molecules 25(20) (2020).
65. E.B. Souto, S. Doktorovová, Solid Lipid Nanoparticle Formulations: Pharmacokinetic and Biopharmaceutical Aspects in Drug Delivery, Liposomes, Part F2009, pp. 105-129.

66. L.K. Puri A, Smith B, Lee JH, Yavlovich A, Heldman E, Blumenthal R. , Lipid-based nanoparticles as pharmaceutical drug carriers: from concepts to clinic, Critical Reviews™ in Therapeutic Drug Carrier Systems 26(6):523-80 (2009).
67. Let's talk about lipid nanoparticles, Nature Reviews Materials 6(2) (2021) 99-99.
68. M.M.S.A.G.W. A. D. BANGHAM, The Action of Steroids and Streptolysin S on the Permeability of Phospholipid Structures to Cations, J. Mol. Biol. (1965) 13, 253-259.
69. X. Yang, X. Zhao, M.A. Phelps, L. Piao, D.M. Rozewski, Q. Liu, L.J. Lee, G. Marcucci, M.R. Grever, J.C. Byrd, J.T. Dalton, R.J. Lee, A novel liposomal formulation of flavopiridol, Int J Pharm 365(1-2) (2009) 170-4.
70. T. Stylianopoulos, EPR-effect: utilizing size-dependent nanoparticle delivery to solid tumors, Therapeutic Delivery 4(4): (2013) 421-423.
71. I.F. Maria Laura, Dosio Luigi Cattel, Stealth liposomes: review of the basic science, rationale, and clinical applications, existing and potential, International Journal of Nanomedicine 2006:1(3) 297–315.
72. R. Kumar, Lipid-Based Nanoparticles for Drug-Delivery Systems, Nanocarriers for Drug Delivery2019, pp. 249-284.
73. M. Sala, K. Miladi, G. Agusti, A. Elaissari, H. Fessi, Preparation of liposomes: A comparative study between the double solvent displacement and the conventional ethanol injection—From laboratory scale to large scale, Colloids and Surfaces A: Physicochemical and Engineering Aspects 524 (2017) 71-78.
74. C.T.R. Sriram Vemuri, Preparation and characterization of liposomes as therapeutic delivery systems: a review, Pharmaceutics Acta Helvetiae 70 (1995) 95-111.
75. O.R. Justo, A.M. Moraes, Kanamycin incorporation in lipid vesicles prepared by ethanol injection designed for tuberculosis treatment, J Pharm Pharmacol 57(1) (2005) 23-30.
76. C. Charcosset, A. Juban, J.-P. Valour, S. Urbaniak, H. Fessi, Preparation of liposomes at large scale using the ethanol injection method: Effect of scale-up and injection devices, Chemical Engineering Research and Design 94 (2015) 508-515.
77. G. Amoabediny, F. Haghiralsadat, S. Naderinezhad, M.N. Helder, E. Akhoundi Kharanaghi, J. Mohammadnejad Arough, B. Zandieh-Doulabi, Overview of preparation methods of polymeric and lipid-based (niosome, solid lipid, liposome) nanoparticles: A comprehensive review, International Journal of Polymeric Materials and Polymeric Biomaterials 67(6) (2017) 383-400.
78. S. Decker, E.A. Sausville, Preclinical modeling of combination treatments: fantasy or requirement?, Ann N Y Acad Sci 1059 (2005) 61-9.
79. D. Lane, Designer combination therapy for cancer, Nature Biotechnology 24 (2006) 163–164.
80. D.G. Pfister, D.H. Johnson, C.G. Azzoli, W. Sause, T.J. Smith, S. Baker, Jr., J. Olak, D. Stover, J.R. Strawn, A.T. Turrisi, M.R. Somerfield, O. American Society of Clinical, American Society of Clinical Oncology treatment of unresectable non-small-cell lung cancer guideline: update 2003, J Clin Oncol 22(2) (2004) 330-53.
81. T. Yang, F.D. Cui, M.K. Choi, H. Lin, S.J. Chung, C.K. Shim, D.D. Kim, Liposome formulation of Paclitaxel with enhanced solubility and stability, Drug Deliv 14(5) (2007) 301-8.
82. T. Negishi, F. Koizumi, H. Uchino, J. Kuroda, T. Kawaguchi, S. Naito, Y. Matsumura, NK105, a Paclitaxel-incorporating micellar nanoparticle, is a more potent radiosensitising agent compared to free Paclitaxel, Br J Cancer 95(5) (2006) 601-6.

83. T.-z.Y. Da-Bing Chen, Wang-Liang Lu, Qiang Zhang, In Vitro and in Vivo Study of Two Types of Long-Circulating Solid Lipid Nanoparticles Containing Paclitaxel, Chemical and Pharmaceutical Bulletin 49(11) (2001) 1444—1447.
84. A.C. Anselmo, S. Mitragotri, Nanoparticles in the clinic: An update, Bioeng Transl Med 4(3) (2019) e10143.
85. C.J. Hitzman, W.F. Elmquist, T.S. Wiedmann, Development of a respirable, sustained release microcarrier for 5-fluorouracil II: In vitro and in vivo optimization of lipid coated nanoparticles, J Pharm Sci 95(5) (2006) 1127-43.
86. Y.C. Kuo, I.W. Chao, Conjugation of melanotransferrin antibody on solid lipid nanoparticles for mediating brain cancer malignancy, Biotechnol Prog 32(2) (2016) 480-90.
87. R. Li, J.S. Eun, M.K. Lee, Pharmacokinetics and biodistribution of Paclitaxel loaded in pegylated solid lipid nanoparticles after intravenous administration, Arch Pharm Res 34(2) (2011) 331-7.
88. M.C. Leiva, R. Ortiz, R. Contreras-Caceres, G. Perazzoli, I. Mayevych, J.M. Lopez-Romero, F. Sarabia, J.M. Baeyens, C. Melguizo, J. Prados, Tripalmitin nanoparticle formulations significantly enhance Paclitaxel antitumor activity against breast and lung cancer cells in vitro, Sci Rep 7(1) (2017) 13506.
89. T.S. Kenya Kamimura, Yasushi Tamura, Masaaki Takamura, Takeshi Yokoo, Masato Igarashi, Hirokazu Kawai, Satoshi Yamagiwa, Minoru Nomoto and Yutaka Aoyagi, Phase I study of Miriplatin combined with transarterial chemotherapy using CDDP powder in patients with hepatocellular carcinoma, BMC Gastroenterology 12:127 (2012).
90. Y. Imai, T. Chikayama, M. Nakazawa, K. Watanabe, S. Ando, Y. Mizuno, K. Yoshino, K. Sugawara, K. Hamaoka, K. Fujimori, M. Inao, N. Nakayama, M. Oka, S. Nagoshi, S. Mochida, Usefulness of Miriplatin as an anticancer agent for transcatheter arterial chemoembolization in patients with unresectable hepatocellular carcinoma, J Gastroenterol 47(2) (2012) 179-86.
91. H. Nishikawa, T. Inuzuka, H. Takeda, J. Nakajima, A. Sakamoto, S. Henmi, T. Ishikawa, S. Saito, R. Kita, T. Kimura, Y. Osaki, Y. Koshikawa, A case of advanced hepatocellular carcinoma with portal vein tumor thrombus refractory to epirubicin that showed marked decrease in tumor markers after transcatheter arterial infusion with Miriplatin, Case Rep Oncol 4(2) (2011) 327-35.
92. S.O. Takuji Okusaka, Toshio Nakanishi, Shigetoshi Fujiyama, Yasuhiko Kubo, Phase II trial of intra-arterial chemotherapy using a novel lipophilic platinum derivative (SM-11355) in patients with hepatocellular carcinoma, Invest New Drugs 22(2):169-76. (2004).
93. S. Fujiyama, J. Shibata, S. Maeda, M. Tanaka, S. Noumaru, K. Sato, K. Tomita, Phase I clinical study of a novel lipophilic platinum complex (SM-11355) in patients with hepatocellular carcinoma refractory to Cisplatin/lipiodol, Br J Cancer 89(9) (2003) 1614-9.
94. S.K.T.N.T.Y.S.F.Y. Takeuchi, In vitro release of SM-11355, cis[((1R,2R)-1,2-cyclohexanediamine-N,N')bis(myristato)] platinum(II) suspended in lipiodol., Biological & Pharmaceutical Bulletin 23(5):637-640 (2000).
95. G.A. Meyer, ICP: still the panacea for trace metals analysis?, Analytical Chemistry 59 (23), 1345A-1354A (1987).
96. J.W. Olesik, Elemental analysis using ICP-OES and ICP/MS, Analytical Chemistry 63 (1), 12A-21A (1991).

97. C. Stoving, H. Jensen, B. Gammelgaard, S. Sturup, Development and validation of an ICP-OES method for quantitation of elemental impurities in tablets according to coming US pharmacopeia chapters, J Pharm Biomed Anal 84 (2013) 209-14.
98. K.F. Khan, Application, principle and operation of ICP-OES in pharmaceutical analysis, Pharma Innovation 8(11):281-282 (2019).
99. S.C. Wilschefski, M.R. Baxter, Inductively Coupled Plasma Mass Spectrometry: Introduction to Analytical Aspects, Clin Biochem Rev 40(3) (2019) 115-133.
100. S.J. Maeda S, Fujiyama S, Tanaka M, Noumaru S, Sato K, Tomita K., Long-term follow-up of hepatic arterial chemoembolization with Cisplatin suspended in iodized oil for hepatocellular carcinoma, Hepato-gastroenterolog 50(51):809-813 (2003).
101. T.-Y.Y. Feng R. Luo , Steven D. Wyrick , Stephen G. Chaney High-performance liquid chromatographic separation of the biotransformation products of oxaliplatin, Journal of Chromatography B 724(2):345-56 (1999).
102. P.M. Mauldin SK, Richard FA, Wyrick SD, Voyksner RD, Chaney SG, Displacement of the bidentate malonate ligand from (d,l-trans-1,2-diaminocyclohexane)malonatoplatinum(II) by physiologically important compounds in vitro, Bioehemiical PharmacoIogy 37(17):3321-33 (1988).
103. J. Shimakura, K. Fujimoto, S. Komuro, M. Nakano, H. Kanamaru, Long-term disposition of a novel lipophilic platinum complex SM-11355 in dog after intrahepatic arterial administration: highly sensitive detection of platinum and radioactivity, Xenobiotica 32(5) (2002) 399-409.
104. S. Liu, Y. Li, X. Wang, J. Ma, L. Zhang, G. Xia, Preparation, Characterization, and Antitumor Activities of Miriplatin-Loaded Liposomes, J Pharm Sci 105(1) (2016) 78-87.
105. D.J. Smith, Chapter 1. Characterization of Nanomaterials Using Transmission Electron Microscopy, Nanocharacterisation2015, pp. 1-29.
106. M. Asadi Asadabad, M. Jafari Eskandari, Transmission Electron Microscopy as Best Technique for Characterization in Nanotechnology, Synthesis and Reactivity in Inorganic, Metal-Organic, and Nano-Metal Chemistry 45(3) (2014) 323-326.
107. L. Graham, J.M. Orenstein, Processing tissue and cells for transmission electron microscopy in diagnostic pathology and research, Nat Protoc 2(10) (2007) 2439-50.
108. V. Bello, G. Mattei, P. Mazzoldi, N. Vivenza, P. Gasco, J.M. Idee, C. Robic, E. Borsella, Transmission electron microscopy of lipid vesicles for drug delivery: comparison between positive and negative staining, Microsc Microanal 16(4) (2010) 456-61.
109. L.A.G. Joachim Mayer, Takeo Kamino, and Joseph Michael, TEM Sample Preparation and FIB-Induced Damage, MRS Bulletin 32(5), 400-407 (2007).
110. I.J. Marina M.Todand, Kym E. Jarvis, Microwave digestion and alkali fusion procedures for the determination of the platinum-group elements and gold in geological materials by ICP-MS, Chemical Geology 124(1-2):21-36 (1995).
111. M. Niemelä, S. Pitkäaho, S. Ojala, R.L. Keiski, P. Perämäki, Microwave-assisted aqua regia digestion for determining platinum, palladium, rhodium and lead in catalyst materials, Microchemical Journal 101 (2012) 75-79.
112. Y. Zhao, Y. Wang, F. Ran, Y. Cui, C. Liu, Q. Zhao, Y. Gao, D. Wang, S. Wang, A comparison between sphere and rod nanoparticles regarding their in vivo biological behavior and pharmacokinetics, Sci Rep 7(1) (2017) 4131.
113. K.Y. Kim, Nanotechnology platforms and physiological challenges for cancer therapeutics, Nanomedicine 3(2) (2007) 103-10.

114.J.K. Patra, G. Das, L.F. Fraceto, E.V.R. Campos, M.D.P. Rodriguez-Torres, L.S. Acosta-Torres, L.A. Diaz-Torres, R. Grillo, M.K. Swamy, S. Sharma, S. Habtemariam, H.S. Shin, Nano based drug delivery systems: recent developments and future prospects, J Nanobiotechnology 16(1) (2018) 71.
115.D.L. Stirland, J.W. Nichols, S. Miura, Y.H. Bae, Mind the gap: a survey of how cancer drug carriers are susceptible to the gap between research and practice, J Control Release 172(3) (2013) 1045-64.
116.B.W. Huang, J.Q. Gao, Application of 3D cultured multicellular spheroid tumor models in tumor-targeted drug delivery system research, J Control Release 270 (2018) 246-259.
117.A. Tchoryk, V. Taresco, R.H. Argent, M. Ashford, P.R. Gellert, S. Stolnik, A. Grabowska, M.C. Garnett, Penetration and Uptake of Nanoparticles in 3D Tumor Spheroids, Bioconjug Chem 30(5) (2019) 1371-1384.
118.M. Kapalczynska, T. Kolenda, W. Przybyla, M. Zajaczkowska, A. Teresiak, V. Filas, M. Ibbs, R. Blizniak, L. Luczewski, K. Lamperska, 2D and 3D cell cultures - a comparison of different types of cancer cell cultures, Arch Med Sci 14(4) (2018) 910-919.
119.Y. Imamura, T. Mukohara, Y. Shimono, Y. Funakoshi, N. Chayahara, M. Toyoda, N. Kiyota, S. Takao, S. Kono, T. Nakatsura, H. Minami, Comparison of 2D- and 3D-culture models as drug-testing platforms in breast cancer, Oncol Rep 33(4) (2015) 1837-43.
120.F. Pampaloni, Reynaud, E. & Stelzer, E. , The third dimension bridges the gap between cell culture and live tissue, Nature Reviews Molecular Cell Biology 8 (2007) 839–845.
121.S. Breslin, L. O'Driscoll, Three-dimensional cell culture: the missing link in drug discovery, Drug Discov Today 18(5-6) (2013) 240-9.
122.N. Chaicharoenaudomrung, P. Kunhorm, P. Noisa, Three-dimensional cell culture systems as an in vitro platform for cancer and stem cell modeling, World J Stem Cells 11(12) (2019) 1065-1083.
123.F. Hirschhaeuser, H. Menne, C. Dittfeld, J. West, W. Mueller-Klieser, L.A. Kunz-Schughart, Multicellular tumor spheroids: an underestimated tool is catching up again, J Biotechnol 148(1) (2010) 3-15.
124.C. Gebhard, C. Gabriel, I. Walter, Morphological and Immunohistochemical Characterization of Canine Osteosarcoma Spheroid Cell Cultures, Anat Histol Embryol 45(3) (2016) 219-30.
125.P.N. S Dhar, K Csoka, J Botling, K Nilsson & R Larsson Anti-cancer drug characterisation using a human cell line panel representing defined types of drug resistance., British Journal of Cancer 74 (1996) 888–896.
126.G.A. Georgiev, D.K. Sarker, O. Al-Hanbali, G.D. Georgiev, Z. Lalchev, Effects of poly (ethylene glycol) chains conformational transition on the properties of mixed DMPC/DMPE-PEG thin liquid films and monolayers, Colloids Surf B Biointerfaces 59(2) (2007) 184-93.